AD-A153 101

EFFECTS OF THE CORONA WIND ON THE

COOLING OF A HORIZONTAL CYLINDER

THESIS

Linn E. Hogue
Major, USAF

AFIT/GA/AA/84D-4

DTIC
ELECTE
APR 2 9 1985
E

DEPARTMENT OF THE AIR FORCE
AIR UNIVERSITY

AIR FORCE INSTITUTE OF TECHNOLOGY

Wright-Patterson Air Force Base, Ohio

85 04 26 005

EFFECTS OF THE CORONA WIND ON THE

COOLING OF A HORIZONTAL CYLINDER

THESIS

Linn E. Hogue
Major, USAF

AFIT/GA/AA/84D-4

EFFECTS OF THE CORONA WIND ON THE

COOLING OF A HORIZONTAL CYLINDER

THESIS

Presented to the Faculty of the School of Engineering

of the Air Force Institute of Technology

Air University

In Partial Fulfillment of the

Requirements for the Degree of

Master of Science in Astronautical Engineering

Linn E. Hogue, B.S., M.S.

Major, USAF

December 1984

Approved for public release; distribution unlimited

Preface

The purpose of this study was to study the effect of the corona wind on the heat transfer from a horizontal cylinder. Although there have been a number of studies of the effect of corona wind on heat transfer, nearly all have involved studying a flat plate. I chose to study the cooling of a cylinder because: (1) analytical models for cylinders are well developed, (2) the geometry lends itself to easier analysis, and (3) the cylindrical model has potentially wide application in the cooling of tubes, wires, pipes, and similar items by using the corona wind.

Although I did a considerable amount of testing and varying parameters, I feel I only scratched the surface of the work that could be done. In particular, developing a model for what effect the corona wind has on local heat transfer coefficients around the cylinder would provide better direction for any future research.

In performing my experimentation and writing this thesis, I received a great deal of help and support from a number of people. I want to thank my advisor, Professor Milton Franke for his initial suggestion of this research and for his continuing patience and suggestions. I also wish to thank Professor James Hitchcock and Captain Wesley Cox for their suggestions and expert advice. In assembling the experimental apparatus and keeping it going, thanks go to Mr. Nick Yardich and his technicians in the laboratory

and to Mr. Carl Shortt and the members of the AFIT
Fabrication Shop.   I also wish to thank my friend, Captain
Henry Baird for his hours of help in preparation of this
report, and all the other members of section GA-84D for
their moral support.   Finally, special thanks go to my wife
Joelle, my daughter Dara, and my son Barrett for their
understanding and patience.

Linn E. Hogue

Table of Contents

List of Figures

List of Symbols

Symbol	Definition	Units
A	Area	ft^2
a	Current	amp
A_e/A_i	Shroud exit to inlet ratio	--
D	Cylinder diameter	in
d_e	Emitter to cylinder distance	in
d_m	Emitter to grid distance	in
d_s	Distance from emitter to exit plane of shroud	in
E	Electric potential, AC	volt
g	Acceleration due to gravity, 32.2	ft/sec^2
Gr	Grashof number, $g\beta\Delta Tx^3/\nu^2$	--
h	Local convection heat transfer coefficient	$Btu/hr\ ft^2\ F$
$\bar{h}$	Average convection heat transfer coefficient	$Btu/hr\ ft^2\ F$
I	Current, AC	amp
k	Thermal conductivity	$Btu/hr\ ft\ F$
L	Cylinder length	in
$\overline{Nu}$	Average Nusselt number, $\bar{h}x/k$	--
P_f	Electric field power	watt
P_h	Low voltage input power to cylinder heating coil	watt
Pr	Prandtl number, Cp/k	--
Q	Heat transfer rate	Btu/hr
R	Electrical Resistance	ohm
T	Temperature	F, R

Symbol	Definition	Units
ΔT	Temperature difference, $T_w - T_a$	F
V	Electric potential, DC	kilovolt (kV)
x	Distance vertical normal to cylinder longitudinal axis	in
y	Distance horizontal normal to cylinder longitudinal axis	in
z	Distance along cylinder longitudinal axis	in
β	Thermal coefficient of volume expansion	1/F
ϵ	Emissivity for radiation	--
μ	Dynamic viscosity	lbm/ft hr
ν	Kinematic viscosity	ft^2/hr
ρ	Fluid density	lbm/ft^3
σ	Stefan-Boltzmann constant, 0.1714×10^{-8}	Btu/hr ft^2 R^4

Subscripts

a	Ambient
c	Convection or convective
e	Emitter or air source
l	Losses through ends of cylinder
m	grid or mesh
o	No field applied
r	Radiation or radiative
t	Total
w	Surface of cylinder

Abstract

Experiments were conducted to determine the effect of the corona wind on the convective heat transfer from a horizontally mounted, heated aluminum cylinder. The cylinder was maintained at ground potential with respect to a positve high voltage emitter. Three types of emitters were used in the testing to create the corona wind: two stretched wires, 0.004 in and 0.0125 in diameter and a 19 point emitter. Tests in the free convection condition and with the emitters at various distances and field voltages up to 15 kV were performed to establish a baseline.

Emitters with and without a metallic mesh grid and a two dimensional wooden shroud were tested in various configurations over a range of electrostatic field conditions. In addition, the velocity of the corona wind in certain configurations was measured and a blown air system was used to simulate the corona wind with uncharged air to compare their respective effects on the convective heat transfer from the cylinder.

Results show that significant increases (up to 6 times) in convective heat transfer were effected. The grid and shroud in various combinations were not as effective in increasing the heat transfer as the emitters alone. The uncharged air was more effective in increasing the heat

transfer than corona wind at the same velocity. The size and type of emitter chosen significantly affected the amount of increase in heat transfer at a particular field voltage.

The parameters varied in the experiments included eletrostatic field voltage, emitter to cylinder spacing, emitter to grid spacing, type of emitter, and shroud spacing and position. The primary techniques for data analysis were an energy balance method and flow visualization with a Mach-Zehnder interferometer.

I. Introduction

A number of experimental studies have been done in the past to examine the effect of an electrostatic field on heat transfer rates. Generally, these studies involved using an electrostatic field to create and accelerate ions and, through contact with a fluid (usually air), create the corona wind, or electric wind.

Background

Some of the earlier studies done by Velkoff (15) and by Velkoff and Marco (14) investigated the effects of electostatic fields on heat transfer from a flat plate. They were the first to show that the corona wind could significantly affect the convective heat transfer from a test article. O'Brien (9) later extended the work to examine the effect of the pressure and composition of the working fluid on the heat transfer from a vertical plate in the presence of an electrostatic field. His work showed the effect of the corona wind cooling occurs with other fluids other than air over a range of pressures. Franke (4) obtained increases in the heat transfer from a vertical plate by inducing vortices on the surface of the plate using an electrostatic field. His analytical work added to the understanding of the action of the electrostatic field near the flat plate. Demorest and Gause (2) examined the effect

1

on electrostatic cooling of a flat plate by varying parameters such as emitter probe spacing and field voltage. They discovered that these parameters can have a significant effect on the corona wind cooling. Ho (6) discovered the relative effect of using electrostatic cooling to improve convective heat transfer under forced convection conditions. Mitchell and Williams (7) investigated the use of electostatic cooling in particular configurations of a horizontal plate and found that there are several parameters which can affect the corona wind cooling.

Although these studies all involved the effect of electrostatic cooling on a flat plate with single or multiple emitters or probes, later work expanded into other areas. The studies of Shannon and Pogson (11) using an accelerating device to enhance the cooling effect of the corona wind on a flat plate showed the possibility of increasing the heat transfer rate even further with the device. Stefkovich (12) studied the effects of corona wind cooling on a vertical flat plate using a grid and two dimensional nozzle to accelerate the corona wind. However, he noticed little change in the heat transfer increase by using these accelerating devices. Reynolds and Holmes (10) investigated the the effect of the corona wind on a finned tube in both free and forced convection. They noted a significant increase in convective heat transfer from the tube if the forced convection rate was low.

2

All of these studies involved testing for the cooling effect, or effect on heat transfer, of the corona wind or an electrostatic field by using various devices or by varying parameters of the particular system. In particular, the studies showed significant increases in convective heat transfer from a flat plate in a variety of configurations can be obtained. But most of them involved testing a flat plate and there are few general conclusions which can be drawn or extended to other geometries.

Objective

The objective of this study was to experimentally examine the effects on convective heat transfer from a right circular cylinder, suspended horizontally in air, using corona wind generated by an electrostatic field between a number of fine wire emitters mounted below the cylinder and the cylinder itself. Further, the effects on heat transfer from this cylinder by accelerating and/or directing the corona wind using a grid and shroud were to be examined. The results of using both unaccelerated and accelerated corona wind on the cylinder would then be compared with the baseline free convective heat transfer and with using non-ionized forced air to simulate the action of the corona wind.

The experimental results were to be obtained by using primarily an energy balance technique and, secondarily, using an interferometer method for qualitative results and

3

flow visualization. Although no attempt to analytically model the complex interactions of the corona wind with the free convective flow around the cylinder was planned, the intent was to make empirical observations which may be helpful in both practical application of these results and with follow-on work which may result in a model of this type of system.

Experimental Approach

The objectives of this experimental study were met by dividing the investigation into the following parts:

1. Measurement of baseline free convection heat transfer rate with ΔT of 50 F and no high voltage DC field applied. Comparison of these results with the predicted values based on an empirical model was included.

2. Measurement of the change in convective heat transfer from the cylinder with high voltage field applied to the multipoint emitter and two different stretched wire emitters with no grid or shroud. All of the emitters were positioned directly below the cylinder. The parameters varied here were emitter spacing and field voltage.

3. Determination of change in heat transfer from the cylinder with one stretched wire emitter and the multipoint emitter with combinations of the grid and shroud to accelerate and direct the corona wind. Parameters varied were emitter spacing, grid spacing, position of the emitter with respect to the shroud, and field voltage.

4

4. Determination of the change in heat transfer using ambient, uncharged air simulating the corona wind at the same velocity. Parameters varied were air source spacing, grid spacing, and air velocity. These results were then compared with the corresponding results from experiments using corona wind.

II. Experimental Equipment

The heat transfer from a horizontal cylinder was investigated primarily using a heat balance method and, to a lesser extent, a Mach-Zehnder interferometer for heat transfer calculations and for flow visualization. The experimental equipment used to conduct these studies included a number of sub-systems such as: (1) heated cylinder, (2) Mach-Zehnder interferometer and camera system, (3) thermocouple system, (4) low voltage AC system, (5) high voltage DC system, (6) emitter devices, (7) grid and shroud assemblies, and (8) blown air system. Each of these systems is discussed in more detail below. Figures 1 and 2 show an overall view of the test apparatus. Example configurations of this test equipment used during testing are shown in Figures 3 and 4.

Heated Horizontal Cylinder

An electrically heated right circular cylinder, 1 in in diameter by 10 in long, was suspended with cotton braided cord in the test section of the Mach-Zehnder interferometer with its longitudinal axis horizontal. The cylinder was constructed in two halves to allow for installation of thermocouples internally. It was then assembled using a flush fitting ring, or "collar", on each end. Figure 5 shows an internal view of the cylinder, while Figure 6 shows a schematic of the internal placement of the 12

6

thermocouples. The cylinder was constructed of 2024 aluminum with the surface machined to a smooth, nearly polished surface. The cylinder had a 3/8 in diameter circular channel along its centerline to allow for the coiled heater element as well as the lead wire for the thermocouples. The cylinder was maintained at electrical ground potential through a connector on its upper surface.

Interferometer and Camera System

A Mach-Zehnder type interferometer with 8 in diameter optics, shown schematically in Figure 7, was used for visualization of the thermal gradients around the circular cylinder. The interferometer used a 100 watt mercury vapor lamp as a light source with a Wratten No. 77A filter, thus producing monochromatic green light with wavelength 5461 Angstroms (10^{-10} meters). A Polaroid Graflex camera with Polaroid Type 42 film was used to photograph resulting fringe patterns.

Thermocouple System

The thermocouple system was used to measure the average cylinder temperature. Twelve copper and constantan thermocouples (fabricated from Type T, 30 gage, teflon coated thermocouple wire) were installed with their hot junctions inside the cylinder within an average distance of 1/16 in below the surface of the cylinder. In addition, another two thermocouples were installed in the test section

7

of the interferometer to record the ambient temperature in the test section. Each of the thermocouples was fabricated using arc welding. The thermocouples installed in the cylinder were covered with "Omegabond 101" adhesive, a thermally conductive but electrically insulating epoxy manufactured by Omega Engineering, Inc. The reference junctions of the thermocouples were immersed in a distilled ice water bath in a Dewar flask. The measurement leads of the thermocouples were connected to a Hewlwett-Packard (HP) 3495A Scanner, part of an Automatic Data System which also included an HP 9835B System Controller and an HP 3455A Digital Voltmeter. This system is shown in Figure 8. The Automatic Data System used the computer program shown in Appendix A, written in Hewlett-Packard BASIC programming language, to sequentially sample each of the thermocouples, measure its voltage, convert it to a temperature reading in both Celsius and Fahrenheit using a Hewlett-Packard conversion algorithm, and compute the average cylinder temperature using a weighted system, and then compute the ΔT between this temperature and the ambient temperature.

Low Voltage AC System

The Low Voltage AC system was used to maintain the cylinder at a constant temperature. Low voltage in this case is a relative term. The actual voltage used in this system was 0-120 VAC. A length of Nichrome wire, 0.0125 in

diameter, sheathed in teflon tubing and shaped into a helical coil, was used as a heater inside the center channel of the horizontal cylinder. This heater was connected to a variable voltage (0-130 Volts), alternating current transformer. The current passing through the heating coil was measured using a Hewlett-Packard 3466A Digital Multimeter, which, when combined with the known resistance characteristics of the heating coil, determined the power input into the cylinder. A schematic of the low voltage heater system is shown in Figure 9.

High Voltage DC System

The high voltage system was used to generate and measure the high voltage electric field in the gap between the emitter and the cylinder. A schematic of the system is shown in Figure 10. The emitter was supplied positive voltage with respect to ground from a high voltage direct current (DC) power supply (0 to 30 kV, 35 milliamps). The electric field potential was measured with a Sensitive Research Corp. electrostatic voltmeter (0-15 kV) connected between the high voltage lead and ground. The current resulting from ion flow from the emitter to the cylinder (or to the grid) to ground was measured with an in-line DC microammeter. All high voltage connections were made with Beldon high voltage wire type 8866, rated for 40 kV DC. The maximum field voltage that was tested was 15 kV due to the measurement limit of the electrostatic voltmeter.

Emitter Devices

Two types of emitter devices were used to generate the high voltage field during testing: a stretched wire and a multipoint emitter (see Figure 11). The stretched wire emitter was simply a length of wire (0.0125 in diameter Nichrome or 0.004 in diameter Chromel) mounted in copper rods and stretched between two mounting brackets. The stretched wire was mounted horizontally so that it was parallel to the longintudinal axis of the cylinder and directly below the cylinder in the test section. Mounting holes in the brackets allowed the stretched wire emitter to be positioned a range of discrete distances with respect to the cylinder without moving the cylinder. In use, the stretched wire emitter was connected directly to the high voltage lead of the high voltage DC power supply.

The multipoint emitter consisted of 19 copper rods (4 in long by 1/8 in diameter) with 1/2 in spacing between them, each with approximately 1/4 in of 0.004 in diameter Chromel wire set in the end and mounted in a copper bus bar which was embedded in a plexiglas holder (see Figure 3). The multipoint assembly was mounted so that each of the copper rods (and their Chromel wires) were perpendicular to the longitudinal axis of the cylinder and mounted directly under the cylinder in the test section. In use, the bus bar of the multipoint emitter was connected directly to the high voltage lead of the high voltage DC power supply.

Shroud and Grid Assemblies

A two dimensional shroud with variable area ratio was used in some tests to direct and accelerate the flow from the emitters. The shroud consisted of two wooden wing-like structures, each 1 1/4 in wide by 13 in long by 3/8 in thick, with rounded leading and trailing edges. The two shroud pieces were mounted parallel to the emitter in the same brackets. Figure 11 is a photograph which shows the shroud mounted. The angle and position of the shroud pieces with respect to the emitter could vary across a considerable range. The entire emitter and shroud could be adjusted with respect to the cylinder at the same discrete distances as the emitter alone.

In addition to the shroud, a grid could be mounted in the same mounting brackets as the emitter. The grid consisted of a 1 in by 12 in rectangular section of aluminum mesh mounted on a rectangular frame of 1/8 in diameter copper rod. The mesh consisted of 29 gage aluminum wire interlaced into squares providing a 0.05 in opening between wires. In use, the grid could be mounted and its position adjusted separately from the emitter or the shroud. It was installed with its flat surface horizontal between the emitter and the cylinder. It was maintained at electrical ground potential on a separate ground lead with a separate DC ammeter than the cylinder.

Blown Air System

A blown air system was used to simulate the air flow, or corona wind, from the stretched wire emittter. The system (see Figure 12) consisted of a large wedge-shaped plenum chamber with a 12 in long by 1/64 in wide slot on its top edge which could be mounted in the mounting brackets in the same relative position as the stretched wire emitter. Compressed air from the AFIT laboratory supply line was introduced into the plenum at two inlets near the bottom to produce an air flow from the slot. The stagnation pressure in the plenum was measured using a Bell and Howell 0-25 psig pressure transducer excited by an HP 6205B Power Supply and the pressure reading taken in volts with an HP 3466A Digital Multimeter.

III. Experimental Procedures

The heat transfer rate from the entire cylinder was determined primarily using an energy balance method and secondarily using an interferometer method. The interferometer method also provided a means of flow visualization of the thermal boundary layer around the cylinder. The test procedures and calibration techniques are described here.

Energy Balance Method

The change of heat transfer rate for the cylinder resulting from the action of the corona wind was determined from the amount of electrical power required to be put into the cylinder heater to re-establish the original temperature difference of 50 F between the cylinder and ambient room temperature. By keeping this ΔT constant, the radiative heat transfer change could be neglected. In addition, the conductive heat transfer away from the cylinder was neglected because there was no significant means of conduction. Thus, by neglecting these, the change in convective heat transfer due to the corona wind was the only means of heat loss and could be measured directly. This method was also used to determine the change in convective heat transfer using the blown air system which simulated the corona wind. This energy balance method was applied to seven test configurations labeled A through H in Figure 13.

13

The specific test procedures for each configuration were the same. Room temperature, relative humidity, and barometric pressure were measured to establish ambient conditions. The cylinder was aligned with the emitter and other components, such as the grid and/or shroud; then the cylinder was aligned with the interferometer light beam using small pointers as well as the number and apperance of the interference fringes. The low voltage AC heater in the cylinder was adjusted to yield a ΔT of 50 F with respect to ambient air in the test section. The heater current was recorded and, when combined with the temperature vs. resistance properties of the heater material, the input power calculated. The high voltage DC field was then adjusted to the desired level. The input heater current was adjusted to re-establish the original ΔT between the cylinder and ambient of 50 F and the system allowed to stablize. A ΔT of 50 F was used for all tests. The current required to establish this new condition was recorded. At this point an interferometer photograph was taken of the stabilized condition. This process was then repeated for each new setting of the high voltage DC field in each particular configuration. To check the reproducibility of results, on three separate occasions, data for a particular configuration was retaken on a different day. The data were nearly identical on each occasion, giving confidence in the the experimental procedures.

14

To model the air flow from the stretched wire emitter
by using the blown air system, the velocity of the corona
wind from the emitter was measured for different emitter
distances and field power settings for which the heat
transfer rate was already known from previous tests. The
measurements were made using an Alnor Velometer, model
6000AP. The blown air system was then adjusted to deliver
the same velocity air flow at the same distance. Again, the
same velometer was used to measure the air velocity. The
heat transfer measurements were then taken and compared with
the corona wind results.

Interferometer Method

This method involved taking photographs of the
interference patterns produced by the Mach-Zehnder
interferometer. As described in the energy balance method,
the cylinder was first aligned with the emitter and the grid
and/or the shroud, and then its mounting frame was adjusted
to align the cylinder (and thus the entire test
configuration) with the interferometer light beam. During
this alignment, the distance, d_e, between the emitter and
the cylinder was measured with precision calipers.
Similarly, d_m, the emitter to grid distance, and d_s, the
emitter to shroud exit plane distance, were precisely
measured during the alignment. Prior to each test, the
interferometer was adjusted to the infinite fringe setting
and the ambient temperature, relative humidity, and

15

barometric pressure were recorded. Once the test configuration was established, the high voltage field was adjusted for the particular data required, and the system was allowed to stabilize. A photograph of the interference fringe patterns was taken using the camera system. Photographs were taken at virtually all data points in all configurations. In some, but not all, a calibration marker was placed in the reference beam of the interferometer to allow quantitative dimensional analysis of the interferometer photographs.

Calibration Techniques

After fabrication, each of the Type T, copper and constantan thermocouples used was calibrated against a Fisher Scientific mercury thermometer. The reference junction of the thermocouple was immersed in an ice bath of distilled water and the measurement junction subjected, along with the mercury thermometer, to a range of temperatures from 32 F to 212 F in distilled water. The thermocouple measurement leads were connected to an HP 3466A Digital Multimeter to read the measurement voltages. All thermocouples measured the same as the mercury thermometer within one degree Fahrenheit under all test conditions.

After the thermocouples were calibrated, they were connected to the HP 3495A Scanner, part of the HP Automatic Data Acquisition System used. The reference junctions of the thermocouples were again immersed in an ice bath and the

16

measurement junctions, along with a mercury thermometer, subjected to the same range of temperatures as before. The Automatic Data Acquistion System was then activated using the computer program written for this experiment (see Appendix A). Again, all thermocouples and the data system yielded the same temperature, within one degree Fahrenheit, as the mercury thermometer.

The low voltage AC heater coil used in the cylinder was calibrated to determine its resistance vs. temperature properties. The coil, a teflon sheathed NiChrome wire with 0.0125 inch diameter, was installed in the cylinder in the configuration used for all testing. The coil was heated by adjusting the AC variable transformer to gradually increase the current through it. The temperature of the coil was measured at the surface of the teflon sheath with a thermocouple. Over a range of temperatures from 70 F (ambient) to 300 F, the coil's resistance, R, was measured using an HP 3466A Digital Mulitimeter. The resistance of the coil was a weak function of temperature, ranging from 35.86 ohms at ambient to 36.18 ohms at 300 F. Since it was such a weak function of temperature (less than 1% variation over the usable range), an average value of 36.00 ohms was used for all P_h calculations.

The ΔT of the cylinder was calculated by the computer program used in the HP 9835B System Controller in the Automatic Data Acquistion System. The cylinder temperature used was actually a weighted average of all 12 thermocouple

17

temperatures in the cylinder. The weighting was: each of the 8 thermocouples installed at either end of the cylinder was computed as 7% of the total, and each of the 4 thermocouples installed in the center of the cylinder was computed as 11% of the total. This weighting was adopted to compensate for the lower temperatures at the ends of the cylinder due to convective losses through the ends. The ΔT was then calculated in the System Controller to be the difference between this weighted average cylinder temperature and the ambient temperature measured by one of the thermocouples installed in the test section.

All meters and other test equipment were calibrated by the Wright-Patterson AFB Precision Measurement Equipment Laboratory or required no calibration.

IV. Data Analysis

The heat transfer rate from the horizontal cylinder was calculated using three methods: an empirical model, an energy balance method, and an interferometer method. Each is described here.

Empirical Model Calculations

An empirical model was used to determine the average free convection heat transfer coefficient, $\bar{h}_o$, for the entire cylinder. In addition, the heat transfer rate for the cylinder was calculated using this model to compare with the experimental results.

From the well-accepted empirical equation for a horizontal cylinder (1:364):

$$\overline{Nu} = 0.525 \left[(Gr)(Pr)\right]^{1/4} \tag{1}$$

where

$$\overline{Nu} = \bar{h}_o D/k \tag{2}$$

thus

$$\bar{h}_o = \frac{k(0.525)\left[(Gr)(Pr)\right]^{1/4}}{D} \tag{3}$$

This is the basis for the empirical model. The calculations for the free convection heat transfer coefficient for the cylinder are shown in Appendix B. The empirical model predictions are discussed further in Chapter V.

Energy Balance Method Calculations

To compare the the effects of testing with the various equipment configurations and field power settings, some measure was needed. The measure used throughout the testing was the dimensionless ratio, $\bar{h}/\bar{h}_o$, defined as the ratio of the average heat transfer coefficient for the cylinder with the electrostatic field applied divided by the average heat transfer coefficient for the cylinder without the field applied. The method for calculating $\bar{h}/\bar{h}_o$ presented here is essentially the method used by Franke (5) as modified by Stefkovich (12).

The expression for the heat transfer rate by convection from the horizontal cylinder is

$$Q_C = \bar{h}A\Delta T \qquad (4)$$

And similarly, for the free convection case

$$Q_{OC} = h_oA\Delta T \qquad (5)$$

By using equations (4) and (5), the ratio Q_C/Q_{OC} is

$$\frac{Q_C}{Q_{OC}} = \frac{\bar{h}A\Delta T}{\bar{h}_oA\Delta T} \qquad (6)$$

Then if the area A and temperature difference T are held constant,

$$\frac{\bar{h}}{\bar{h}_o} = \frac{Q_C}{Q_{OC}} \qquad (7)$$

The heat transfer rate at any time can be written as

$$Q_C = Q_{OC} + \Delta Q_C \qquad (8)$$

Substituting equation (8) into equation (7) gives

$$\frac{\bar{h}}{\bar{h}_o} = 1 + \frac{\Delta Q_c}{Q_{oc}} \tag{9}$$

Either equation 10 or 12 can be used to calculate $\bar{h}/\bar{h}_o$. The total heat transfer rate from the cylinder is given by

$$Q_t = Q_{oc} + Q_{col} + Q_r \tag{10}$$

Then the change in total heat transfer rate for the cylinder from free convection to the field applied convection is given as

$$\Delta Q_t = \Delta Q_c + \Delta Q_{cl} + \Delta Q_r \tag{11}$$

If the changes in convective heat transfer rate from the ends, ΔQ_{cl}, and the changes in radiative heat transfer, ΔQ_r, are small, then

$$\Delta Q_t = \Delta Q_c \tag{12}$$

Under steady state conditions, the total heat transfer rate from the cylinder is equal to the electrical power input by the heater coil. This energy is found by measuring the current put into the heater and by combining this with the known resistance of the coil using the relation

$$Q_t = P_h = I^2 R \tag{13}$$

Now it follows that the the change in total heat transfer rate is equal to the change in cylinder heater input power, P_h. Using this and equation (11) gives

$$\Delta Q_t = \Delta P_h = \Delta Q_c \tag{14}$$

Substituting equations (5) and (13) into equation (9) yields

$$\frac{\bar{h}}{\bar{h}_o} = 1 + \frac{\Delta P_h}{\bar{h}_o A \Delta T} \tag{15}$$

21

Where the input power to the heater coil in free convection, P_{ho}, is assumed to be

$$P_{ho} = \bar{h}_o A \Delta T \qquad (16)$$

Then substituting this into equation (15) yields

$$\frac{\bar{h}}{\bar{h}_o} = 1 + \frac{\Delta P_h}{P_{ho}} \qquad (17)$$

Equation (17) is the basis for the experimental calculation of the ratio $\bar{h}/\bar{h}_o$ for all experiments in this study.

Interferometer Method Calculations

A travelling microscope, accurate to 0.001 cm, was used to measure the distance from the surface of the cylinder to the first three interference fringes in an interferometer photograph. Fringes were measured at seven positions radially around the cylinder at 45 degree intervals. Considering vertically upward as zero and measuring clockwise, the first measurement station was at the 45 degree position and the last at 315 degrees. The straight up position could not be measured because the fringes in that position were blocked in the photograph and also were greatly elongated by the upward flow. O'Brien's computer program (9) was modified considerably to enable using two coordinate measurements to get a radial distance from the cylinder. It was further modified to run in BASIC computer language on an 8-bit microprocessor to calculate the heat transfer coefficients and gradients around the cylinder. The computer program is listed in Appendix C. The heat

22

transfer calculations for the interferometer were limited to the free convection condition. Sample results from the computer program are shown in Figure 34. With field power applied, the interference fringes were not usable for calculation. The results from the interferometer calculation are further discussed in Chapter V.

V. Results and Discussion

Baseline Free Convection Heat Transfer

The heat transfer rate for the horizontal cylinder in free convection with no electrostatic field applied was measured by the interferometer method to be 15.68 Btu/hr (4.60 watts) with an ambient temperature of 71 F and a cylinder temperature of 121 F for a ΔT of 50 F. A sample of the interferometer results is given in Appendix C. Under the same conditons the amount of power required to be put in by the heater coil was 16.76 Btu/hr (4.91 watts). This compares very well with the empirical model prediction (see Appendix B) of 16.53 Btu/hr (4.84 watts).

From the empirical model prediction, Q_{col}, the convective heat transfer from the ends of the cylinder, is 0.229 watts, or 4.7% of the total heat transfer and Q_r, the radiative heat transfer, is 0.275 watt, or 5.7% of the total. The convective heat transfer is the majority of the total heat transfer, since it is 89.6% of the total.

Measurements for the Stretched Wire and Multipoint Emitters

The first test configurations used were the two stretched wire emitters (0.004 in diameter Chromel and 0.0125 in diameter Nichrome) and the multipoint emitter without the grid or the shroud. These are configurations A and B in Figure 13. Figures 14, 15, and 16 show plots of the $\bar{h}/\bar{h}_o$ vs. field voltage for all three emitters at various

24

emitter distances, d_e. Note that the shapes of the curves with different emitters are very similar. The primary difference in the results is due to the lower breakdown voltage for the multipoint emitter and thinner stretched wire emitter. The breakdown voltage is the field voltage at which current first begins to flow and form the corona wind. The lower breakdown voltage for the multipoint emitter and smaller diameter stretched wire emitter is due to the higher electrostatic field intensity per unit area on the emitter surface caused by its smaller surface area at the same field voltage.

Figure 17 shows the effects of the corona wind on the cylinder created by the 0.004 in diameter Chromel stretched wire emitter. No effect on the thermal boundary layer was noted until the breakdown field voltage was reached and current began to flow between the emitter and the cylinder. The corona wind can be seen at the higher field voltages as a thin stream impinging on the bottom of the cylinder. The boundary layer appears to separate at approximately the maximum width of the cylinder. The wake above the cylinder assumed a closed oval shape typical of the results for all of the stretched wire emitter tests. The emitter itself can not be seen directly in the photographs because the bracket holding it blocks it from view.

The effect on $\bar{h}/\bar{h}_0$ when varying field input power at varying emitter distances, d_e, with the thin (0.004 in diameter) stretched wire emitter is shown in Figure 18. For

this emitter, the effect on $\bar{h}/\bar{h}_o$ was virtually independent of the emitter spacing; it depended only on the input field power. Figure 19 presents the relationship between field current and input field voltage for this emitter at three emitter distances.

For the multipoint emitter, the effect on the thermal gradients was clearly different from that of the stretched wire emitter as shown in the interferometer photographs in Figure 20. Although the thermal gradients near the cylinder are relatively undisturbed, the outer gradients fan out across the field of view with increasing field voltage, indicating the corona wind from the multipoint emitter is more turbulent and less directional than with the stretched wire emitter. This same effect was noted by Stefkovich (12:17-18) and he explained it as being caused by increased ion concentration.

For the multipoint emitter, the effect on $\bar{h}/\bar{h}_o$ from varying input field power is shown in Figure 21 for the same three distances as for the stretched wire emitter. Again, for the multipoint emitter, the effect on $\bar{h}/\bar{h}_o$ is almost independent of the emitter distance, and depends only on the input field power. The relationship between field current and input field voltage for the multipoint emitter is shown in Figure 22.

By comparing Figures 18 and 21, it can be seen that at any emitter distance, the multipoint emitter produces a

higher value of $\bar{h}/\bar{h}_0$ than the stretched wire emitter at the same field voltage. Figure 23 indicates this more directly by showing $\bar{h}/\bar{h}_0$ versus field voltage for the same value of d_e, 0.75 in, for both the multipoint and stretched wire emitter.

Measurements with Combinations of the Grid and Shroud

Configurations C, D, and E in Figure 13 were tested to determine the effects on the convective heat transfer rate from the horizontal cylinder by using a non-conductive wood shroud and a metallic mesh grid to accelerate and direct the corona wind from the stretched wire and multipoint emitters. Note that throughout the remaining discussion, the stretched wire emitter referred to will be the 0.004 in diameter Chromel stretched wire emitter unless specifically noted otherwise.

The initial configuration tested was the stretched wire emitter with the shroud alone. During preliminary testing, it was discovered that the non-conductive wooden shroud significantly inhibited the electrostatic field, that is it acted as a dielectric to prevent field current flow and thus kept the corona wind from forming except at much higher breakdown voltage. The only solution was to move the shroud farther away from the emitter and the grounded cylinder. However, the physical parameters of the test equipment used limited the amount of spacing between them that could be attained. Figure 24 shows a plot of $\bar{h}/\bar{h}_0$ versus field

27

voltage for a successful run with the stretched wire emitter and the shroud alone. In this case, the stretched wire emitter is positioned at the exit plane of the shroud. For comparison, data for the same conditions from the baseline case without the shroud is shown on the same Figure. It can be seen that with field power higher than about 0.5 watt, there is virtually no effect on the convective cooling due to the presence of the shroud. This result and the difficulty in obtaining useful data with the shroud alone limited the testing of this configuration. Instead, a configuration with the grid alone or both the shroud and grid was used.

The stretched wire emitter was tested using both the shroud and the grounded grid in various configurations. Figure 25 is a series of interferometer photographs for one of these configurations at various field voltages which shows a typical pattern of corona wind development. Comparison with Figure 17 for the no shroud and grid baseline case, shows that with the shroud and grid, the boundary layer at the bottom of the cylinder is compressed in the same manner and also that the boundary layer separates at about the maximum width of the cylinder. However, the wake above the cylinder expands away from the cylinder more than with the emitter alone. An explanation for this is that the grid, since it is grounded, removes most of the ions from the corona wind, so that the air is

28

essentially neutrally charged when it flows around the cylinder. This uncharged air is not attracted to the grounded cylinder like the charged air in the corona wind is and does not adhere as closely to the cylinder.

However, these differences in the visualization of the thermal gradients did not significantly affect the cooling effect of the corona wind, even after altering some of the parameters of the configuration. For example, testing was done with a d_e (distance from emitter to cylinder) of 1.0 in and a d_m (distance from emitter to grid) of 0.75 in, leaving a cylinder to grid distance of 0.25 in with the emitter 0.25 in behind the exit plane of the shroud. The configuration was then changed with the emitter 0.75 in behind the exit plane of the shroud, but with the same d_e and d_m which meant the grid was at the exit plane of the shroud. Data were then taken in this configuration. Another change was made to move the cylinder to approximately 1/32 in above the grid, but leaving the emitter, grid, and shroud positions unchanged. The effects of all these configurations on $\bar{h}/\bar{h}_o$ versus field voltage is shown in Figure 26. As can be seen from this figure, there was very little, if any, effect on convective heat transfer from the cylinder by changing these parameters with the stretched wire emitter. What effect was noted was a slight decrease in $\bar{h}/\bar{h}_o$ from the baseline case with no grid or shroud.

Similar results were obtained for the multipoint emitter with the same configurations given above, except

that the decrease in corona wind cooling from the baseline case of no grid or shroud was more noticable. Figure 27 shows the results of the same configurations for the multipoint emitter as Figure 26 does for the stretched wire emitter. Again, the baseline case of the multipoint emitter with no grid or shroud was plotted as a reference. Note in Figure 27 that the emitter alone yielded a higher $\bar{h}/\bar{h}_o$ than any of the shroud and grid configurations.

As a general observation, in all of the testing with the grid and shroud, a markedly increased tendency of arcing from the emitter to the grid at relatively low field voltages (10-12 kV) was noted. This is due to the increased ion concentration in the volume of air confined by the shroud and by the lower breakdown voltage of the small diameter wires on the grid. Additionally, when using the 0.004 in diameter stretched wire emitter with the grid, the wire would begin violent vibration above approximately 10 kV and, if allowed to continue, would break the wire. One interesting observation was that, when testing with the grid, there was very little current flow from the emitter to the grounded cylinder, usually no more than 3% of the total field current. This meant that the grid was attracting the large majority of the ions and few were passing through. However, there was still a very significant cooling effect on the cylinder from the air that did pass through, in fact, not much less than without the grid. This implies that the

corona wind could still be used to cool non-conductive objects as suggested by Velkoff and Kulacki (13).

Further testing was done to investigate the effect on corona wind cooling by using the grid alone, since the grid and shroud did not seem to be particularly effective. The stretched wire emitter was used with the grid mounted between the emitter and the cylinder. As an example of the results, refer to Figure 28. The stretched wire was tested with d_e equal to 1.0 in, with d_m equal to 0.5 in and later equal to 0.75 in. The results of the baseline case of no grid or shroud with a d_e of 1.0 in were also put on the figure for comparison. As the figure shows, neither configuration with the grid gave as high an increase in convective heat transfer rate as the baseline case without the grid, however the differences are small.

Using the multipoint emitter with the grid only gave similar results. Figure 29 is a plot of $\bar{h}/\bar{h}_o$ versus field voltage for the configuration with the multipoint emitter; with d_e of 1.0 in and a d_m of 0.75 in. Along with it is the multipoint emitter with d_e of 1.0 in and no grid. It can be seen again that having the grid between the emitter and cylinder produced smaller increases in convective heat transfer than the emitter alone. However, as noted earlier, there was still significant cooling (nearly as much as without the grid) by the corona wind with very little field current flow to the cylinder.

The results of this section can generally be summarized

by pointing out that in all configurations of testing the convective heat transfer increases from this horizontal cylinder, the emitter alone, whether stretched wire or multipoint, produced an $\bar{h}/\bar{h}_o$ at least equal to, and usually higher than, the same emitter with any combination of grid and shroud at the same input field power. However, when using the grid in any configuration, yielded significant heat transfer increases with little, if any, current flowing to the cylinder.

Measurements of Corona Wind Velocity and Comparison with Uncharged Air

The final objective was to compare the effects of the corona wind on convective cooling of the cylinder with the cooling produced by uncharged air blown in a manner to simulate the corona wind. First the velocity of the corona wind was measured at emitter distances and field power settings at which $\bar{h}/\bar{h}_o$ had already been experimentally determined. The blown air system was then adjusted to yield the same velocities and the $\bar{h}/\bar{h}_o$ determined with this configuration. This then allowed the comparison of the cooling effects of the corona wind and the blown, uncharged air.

The stretched wire emitter (0.004 in diameter) was used in two configurations to measure for the velocity of the corona wind from the emitter to the cylinder. The first was with the grid between the emitter and the velometer probe;

32

the second was with the velometer probe directly over the emitter. The velocities were measured at field voltages corresponding to those used earlier in corona wind tests. These velocities were then duplicated in the blown air system, described in Chapter II, by again measuring them with the velometer and then testing the convective cooling caused by this uncharged air blowing on the cylinder.

The results showed, as in Figures 30, 31, and 32, that with no grid, the uncharged air generally produced a higher $\bar{h}/\bar{h}_o$ than the corona wind at the same velocity. However, in at least the case of d_e equal to 0.75 in (Figure 31), the comparison was quite close. Note that in this testing, d_e refers to either the emitter-to-cylinder distance or the air source to cylinder distance.

With the grid between the emitter (or air source) and the cylinder, the same conclusion is reached, as can be seen from Figure 33. Here the cylinder is only 1/32 in above the grid and the blown air still produced a higher $\bar{h}/\bar{h}_o$ at the same velocity as the blown air produced.

VI. Conclusions

Based on the results of this study, the following conclusions can be drawn:

1. Significant increases in the convective heat transfer rate from a horizontal cylinder can be obtained by using the corona wind for cooling. Under some conditions, increases of more than six times the free convection condition were realized.

2. The corona wind was present only when there was electrostatic field current flow. This substantiates earlier work and reinforces the idea of ions accelerated by the Coulomb force entraining air to create the corona wind.

3. Use of a grid and shroud to accelerate and direct the corona wind resulted in either no increase or a smaller increase in convective heat transfer than with the emitter alone. Additionally, the presence of the non-conductive wood shroud inhibited the electrostatic field and the formation of the corona wind. Use of the grid alone was more effective than use of the grid and shroud together.

4. The corona wind produced a lower increase in the heat transfer rate than non-ionized air at the same velocity. The highest velocity measured was 660 ft/min (11 ft/sec).

5. Significant increases in the convective heat transfer rate were still present with the grid alone with little or no current flow to the cylinder. This confirms

34

the possiblity of corona wind cooling of non-conductive articles as mentioned by Velkoff and Kulacki (13).

6.   Emitter size and configuration significantly affected the convective heat transfer rate increases produced by the corona wind. The multipoint emitter had the lowest breakdown voltage, followed by the 0.004 in diameter stretched wire, and the 0.0125 in diameter stretched wire having the highest breakdown voltage. This difference then affected the amount of increase in convective heat transfer at the same field voltage with all other parameters held constant. Over the range tested, lower breakdown voltage produced higher increases in convective heat transfer as well as higher field current at the same field voltage.

VII. Recommendations

The corona wind cooling of a cylinder should be investigated further to better understand its effects. This investigation, however, should include:

1.   Development of an analytical model of the interaction of the corona wind with the cylinder, with applicability to other geometries and test articles. This would give better direction to further experiments and would also provide some predicted results to compare with the experimental results.

2.   Redesigned instrumentation which would allow better determination of local heat transfer coefficients and would probably contribute to the development of the model mentioned above.

3.   Multiple emitter designs should be tested. This type of configuration would provide a broader, parallel flow type corona wind easier to compare with the analytical models for forced convection over cylinders.

4.   Further explore the configurations described in this study.

FIGURES

Figures 1-33

(1) Test Section with Horizontal Cylinder
(2) Mach-Zehnder Interferometer
(3) Electrostatic Voltmeter (0-30 kV DC)
(4) Ice Bath for Thermocouples
(5) Polaroid Graflex Camera for Taking
    Interference Photographs

Figure 1.   Overall Photograph of Interferometer and Test Section
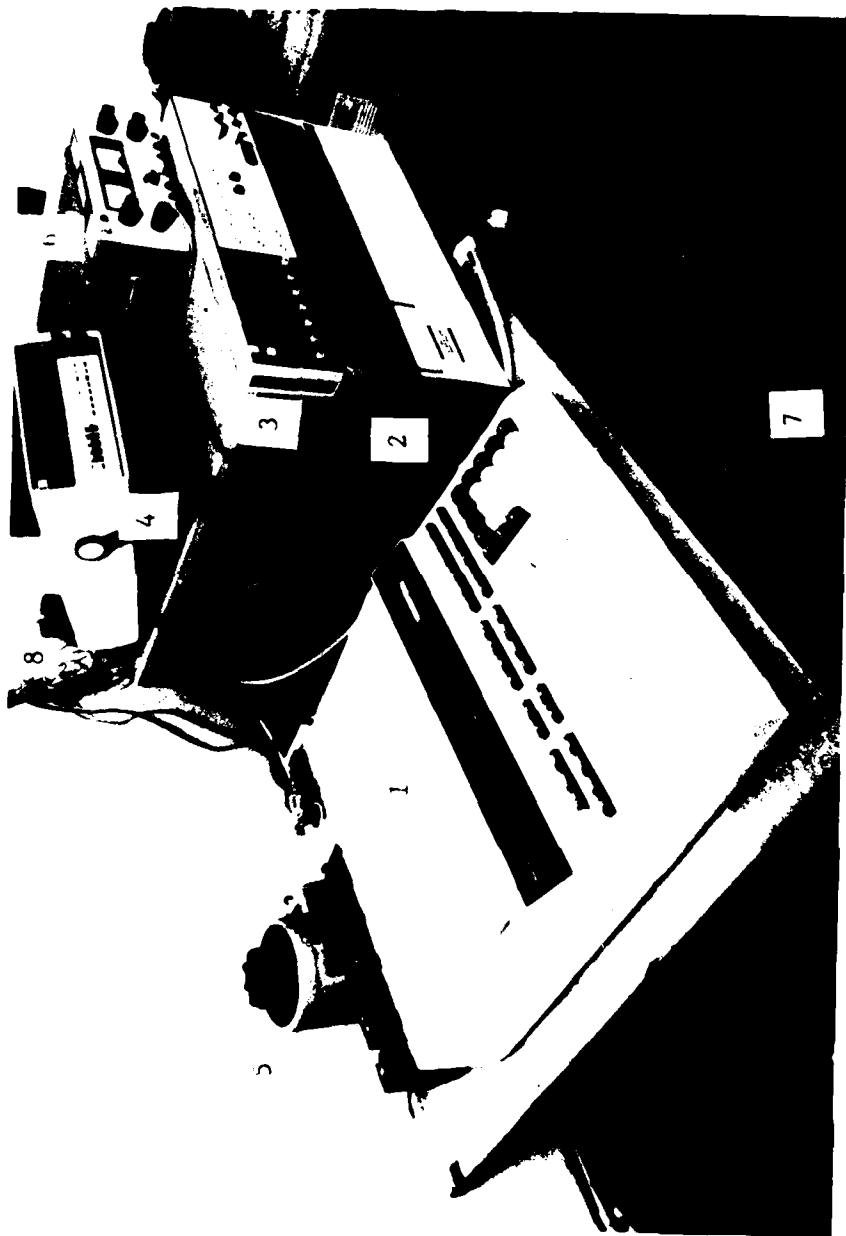
(1) HP 9835B System Controller   (5) Variable AC Transformer
(2) HP 3495A Scanner   (6) HP 6205B Dual Power Supply
(3) HP 3455A Digital Voltmeter   (7) High Voltage DC Power Supply
(4) HP 3466A Digital Multimeter   (8) Ice Bath for Thermocouples

Figure 2. Overall Photograph of Test Equipment

Figure 3. Photograph of Cylinder in Test Section with Multipoint Emitter Installed
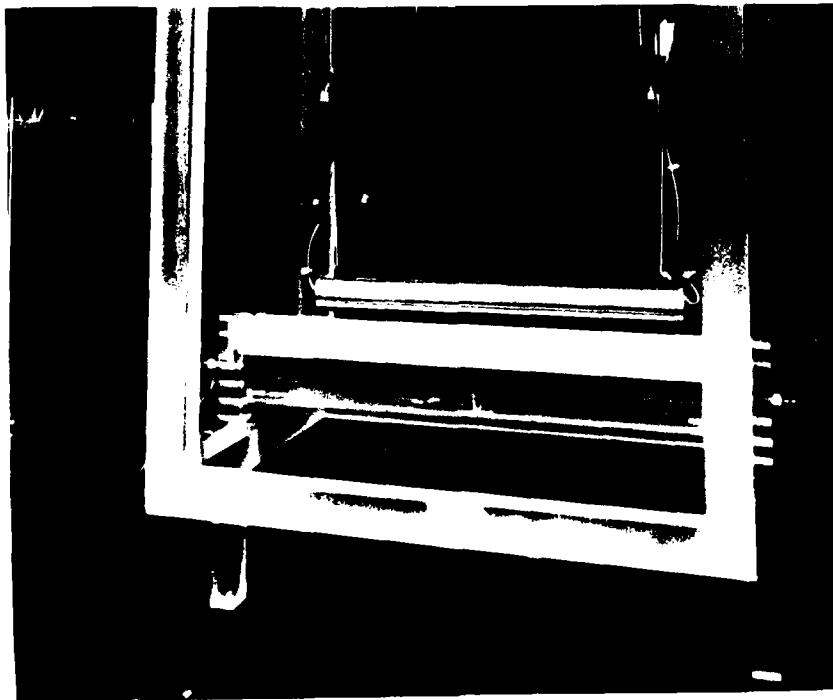
Figure 4. Photograph of Cylinder in Test Section with Shroud Installed

40

Figure 5.   Photograph of Internal View of Cylinder
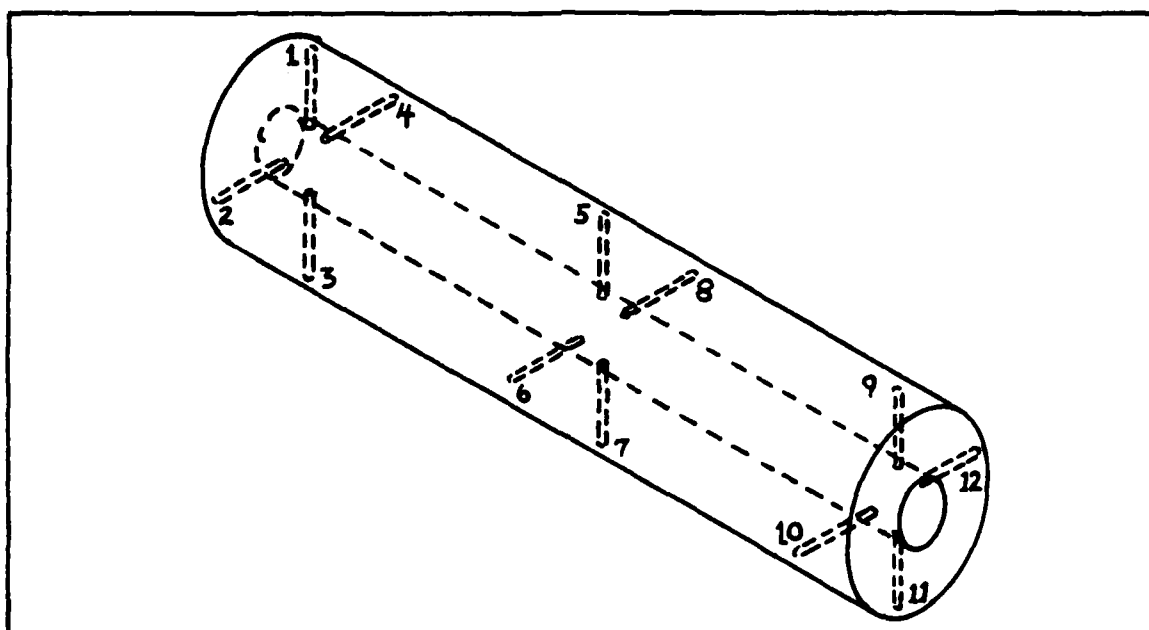
Figure 6.   Schematic Diagram of Thermocouple Placement
Inside the Cylinder
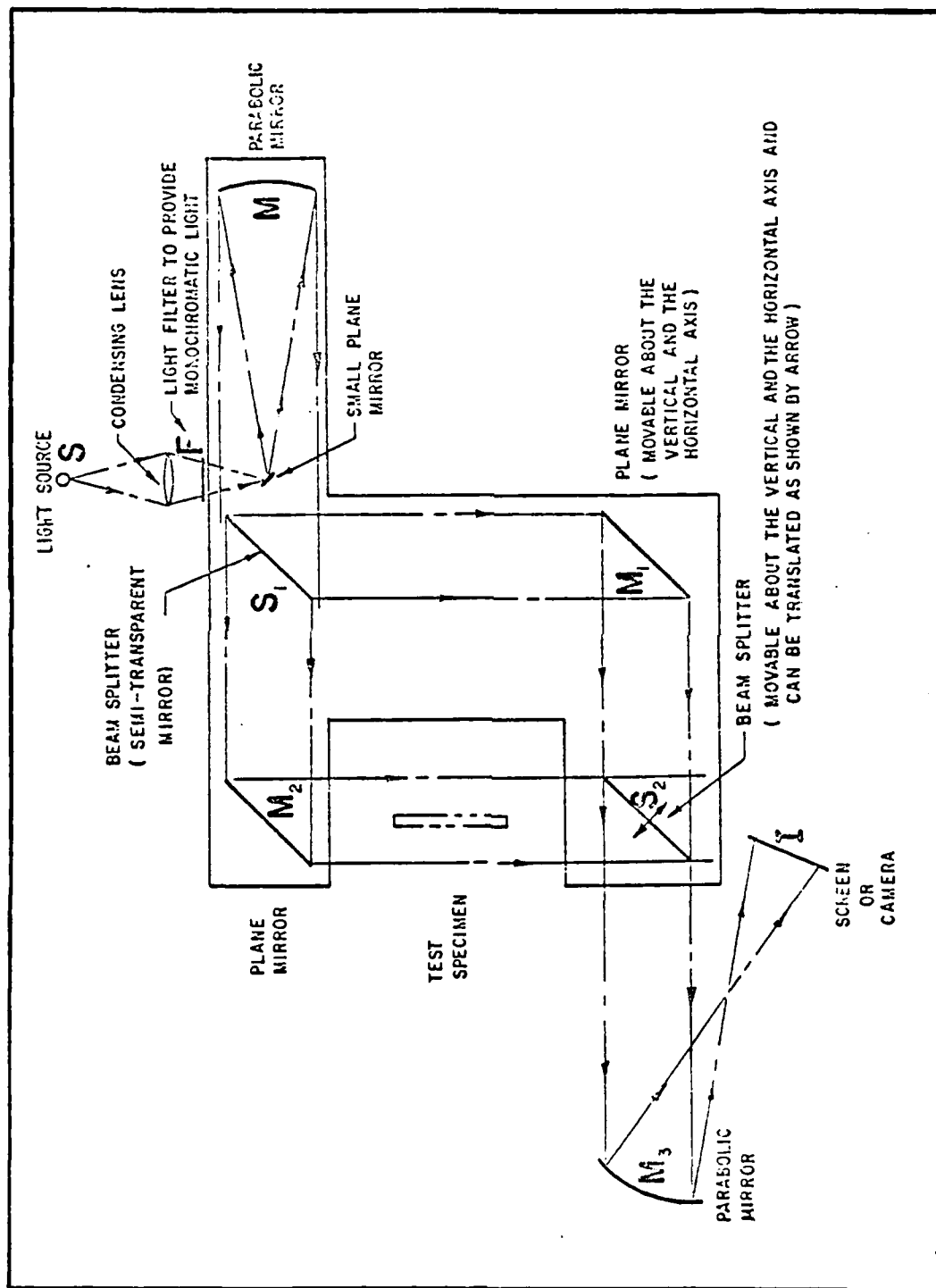
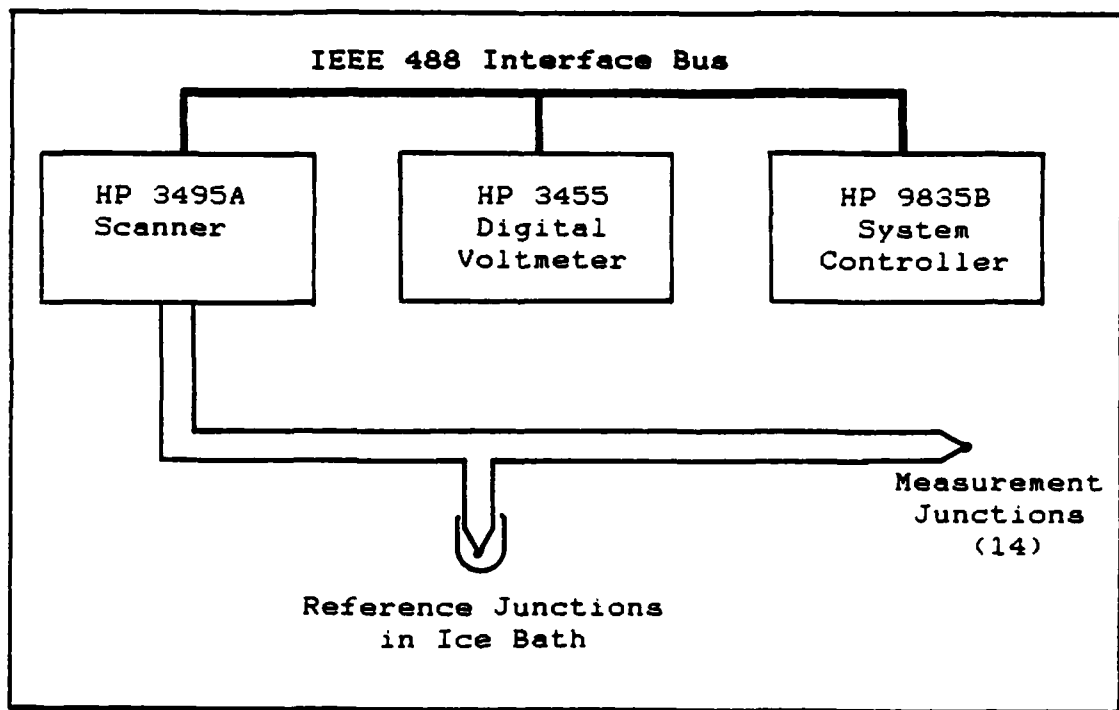Figure 7. Schematic Diagram of Mach-Zehnder Interferometer

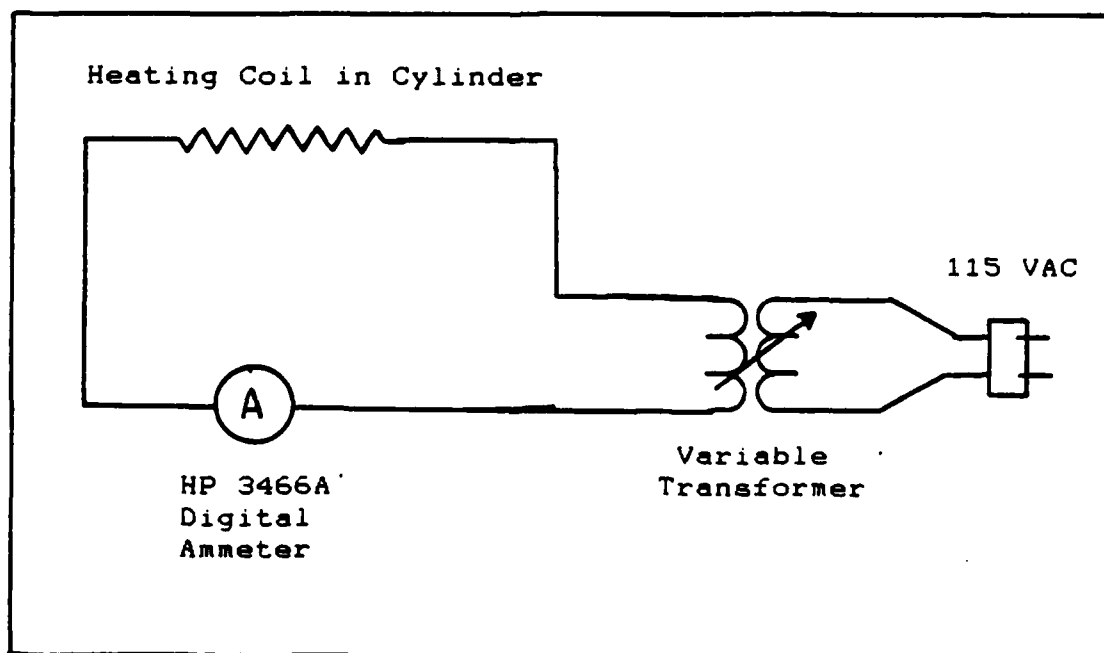Figure 8. Schematic Diagram of Thermocouple System

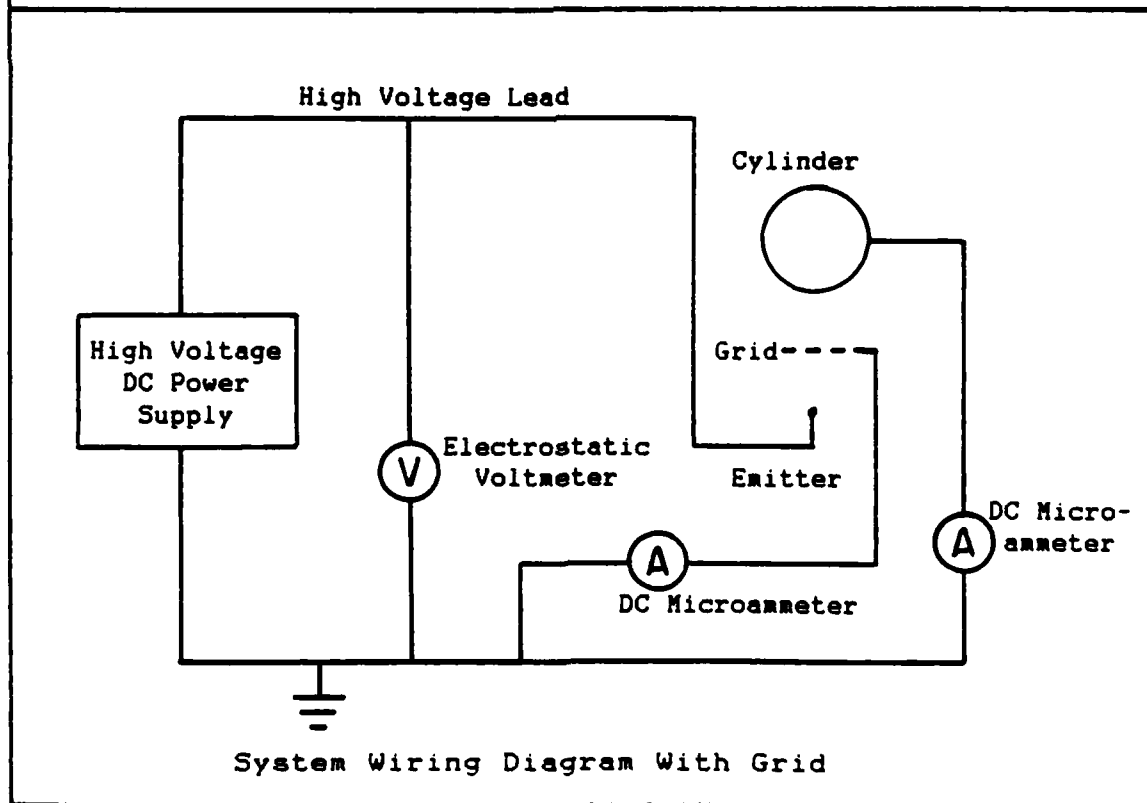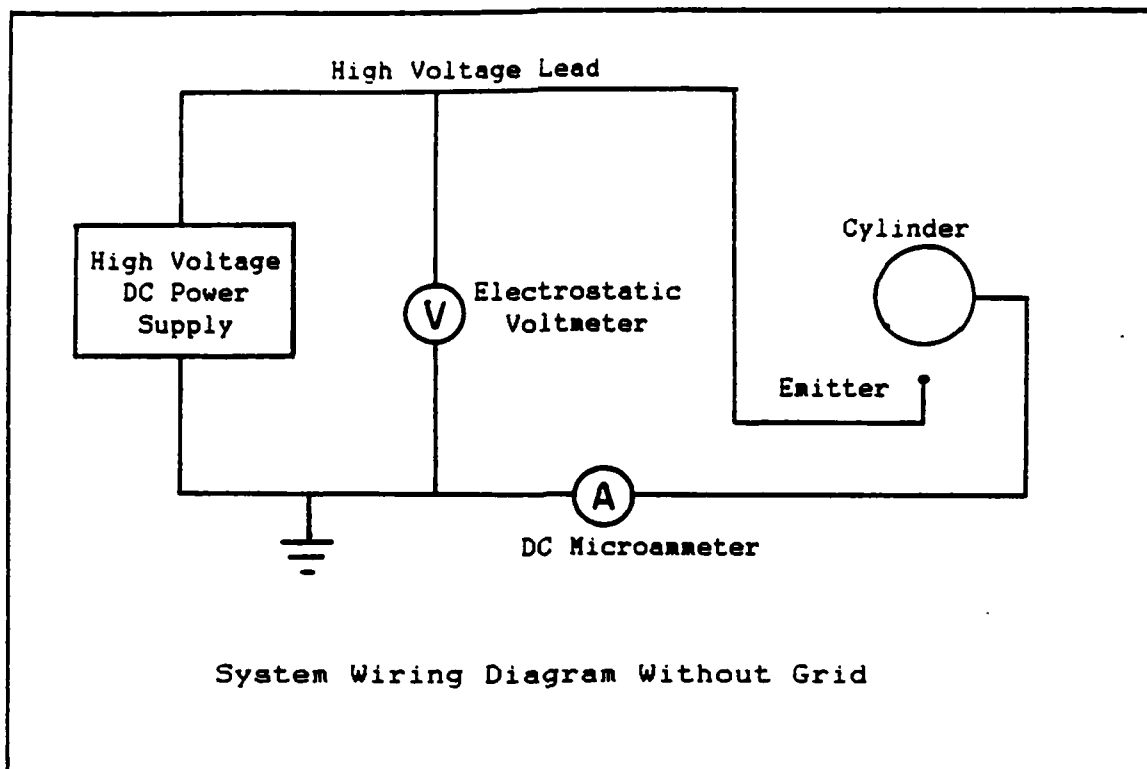Figure 9.   Low Voltage AC Heater System
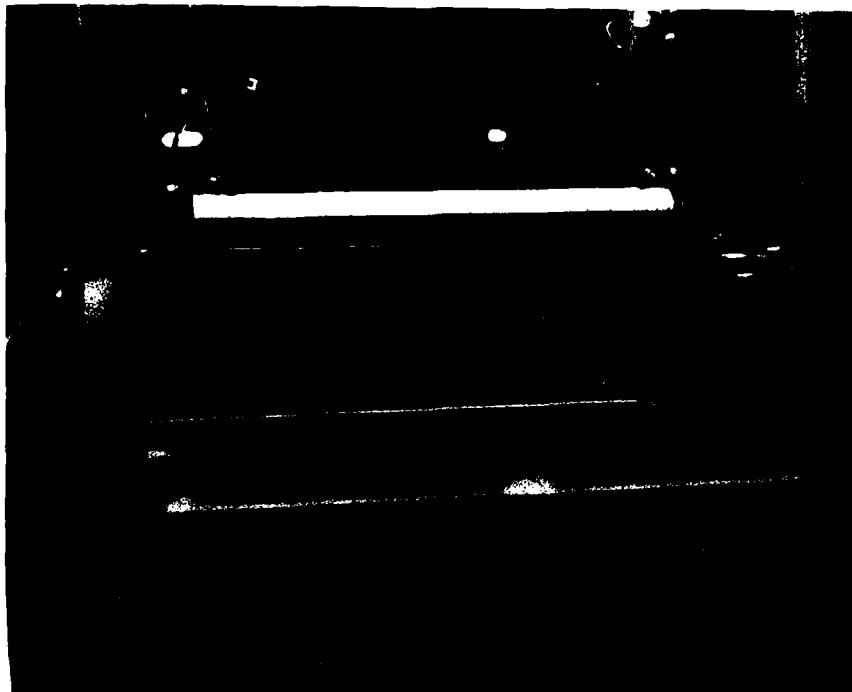
Figure 10. High Voltage DC System

Figure 11. Photograph of Cylinder in Test Section with Stretched Wire Emitter and Grid Installed

Figure 12. Photograph of Cylinder in Test Section with Blown Air System Installed
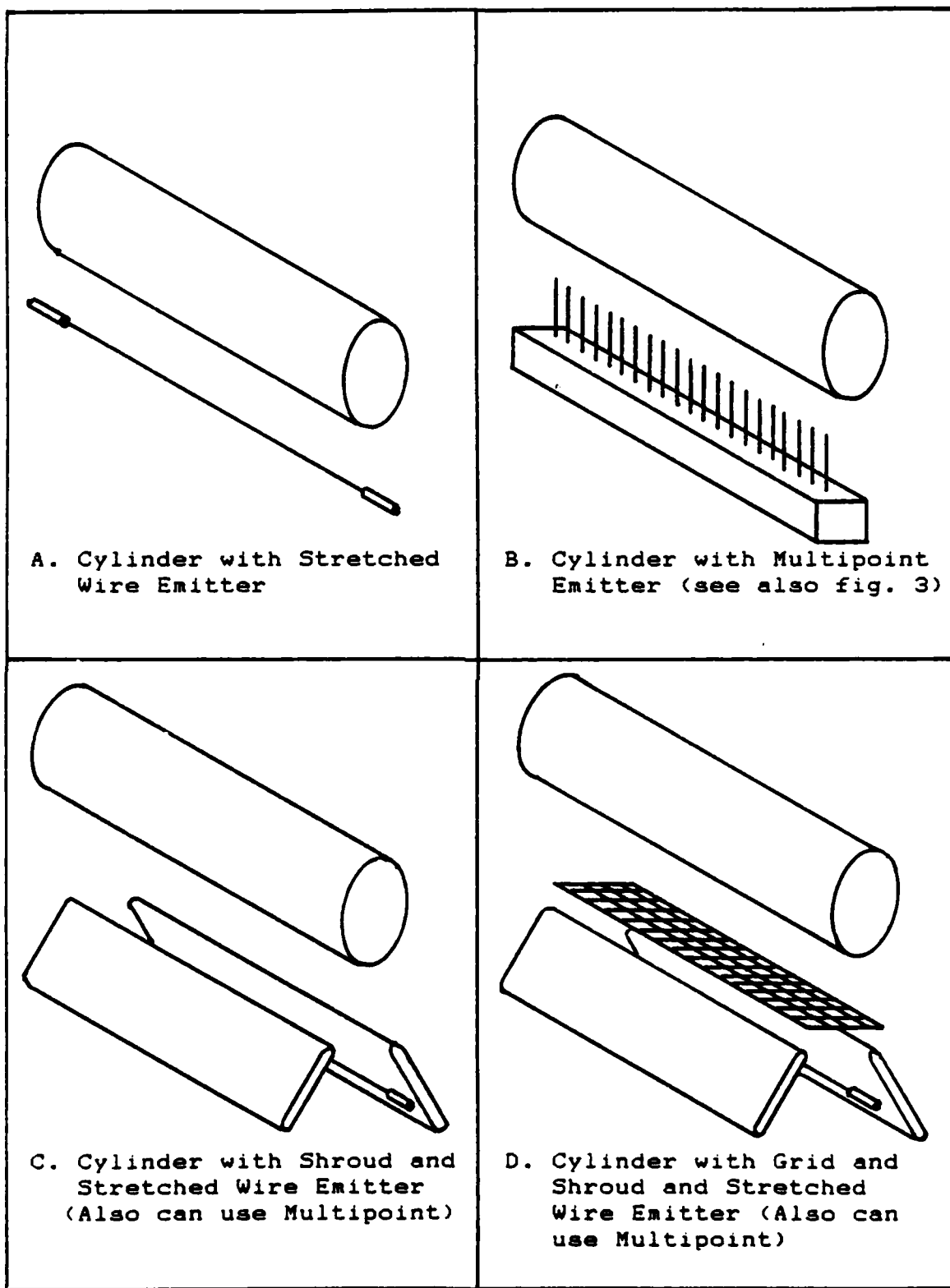
A. Cylinder with Stretched
   Wire Emitter

B. Cylinder with Multipoint
   Emitter (see also fig. 3)

C. Cylinder with Shroud and
   Stretched Wire Emitter
   (Also can use Multipoint)

D. Cylinder with Grid and
   Shroud and Stretched
   Wire Emitter (Also can
   use Multipoint)

Figure 13. Diagrams of Test Configurations

E. Cylinder with Grid and
   Stretched Wire Emitter
   (Also can use Multipoint)

F. Cylinder with Blown Air
   System

G. Cylinder with Grid and
   Blown Air System

Cylinder

Grid

d_e

d_s

d_m
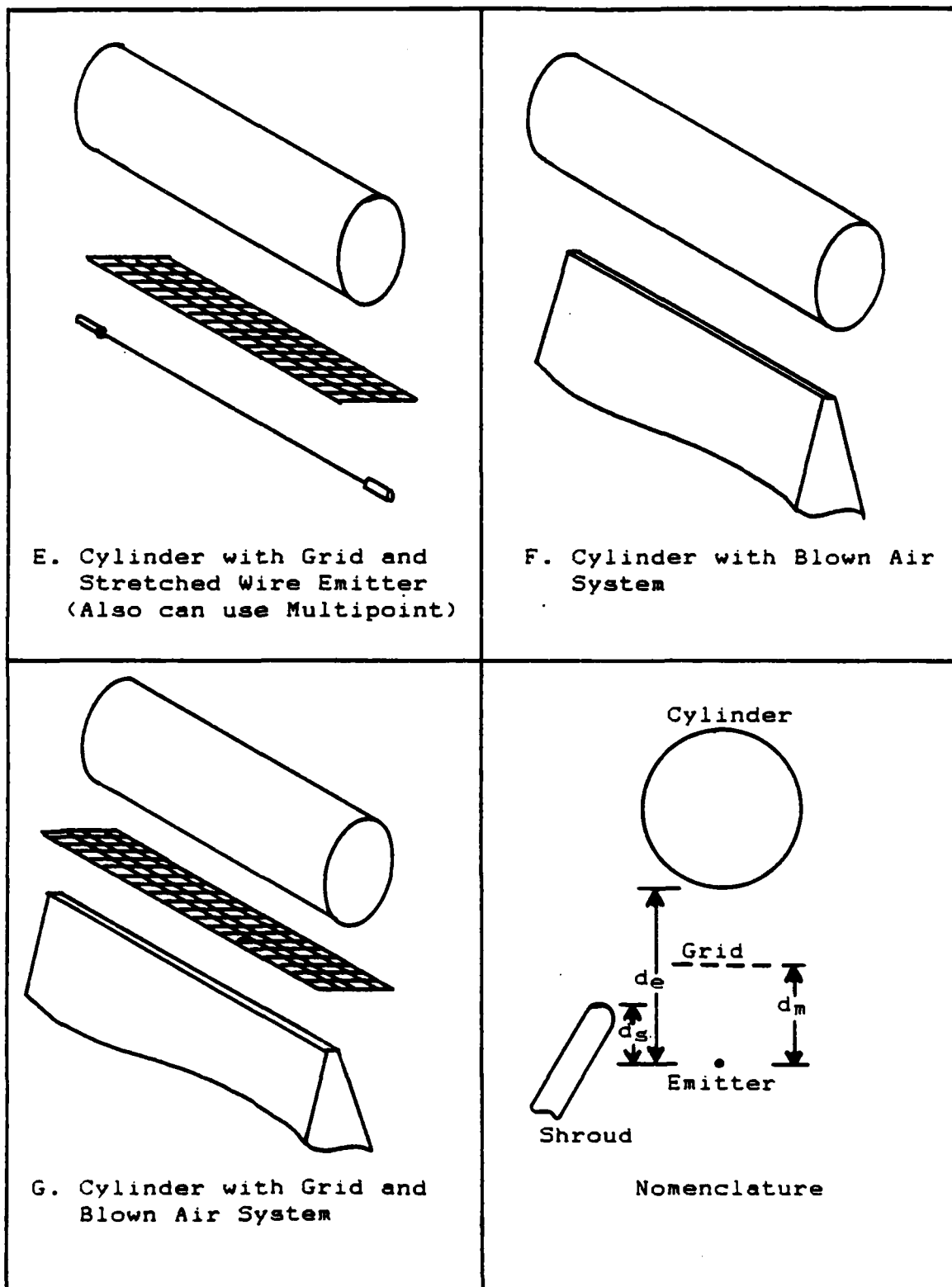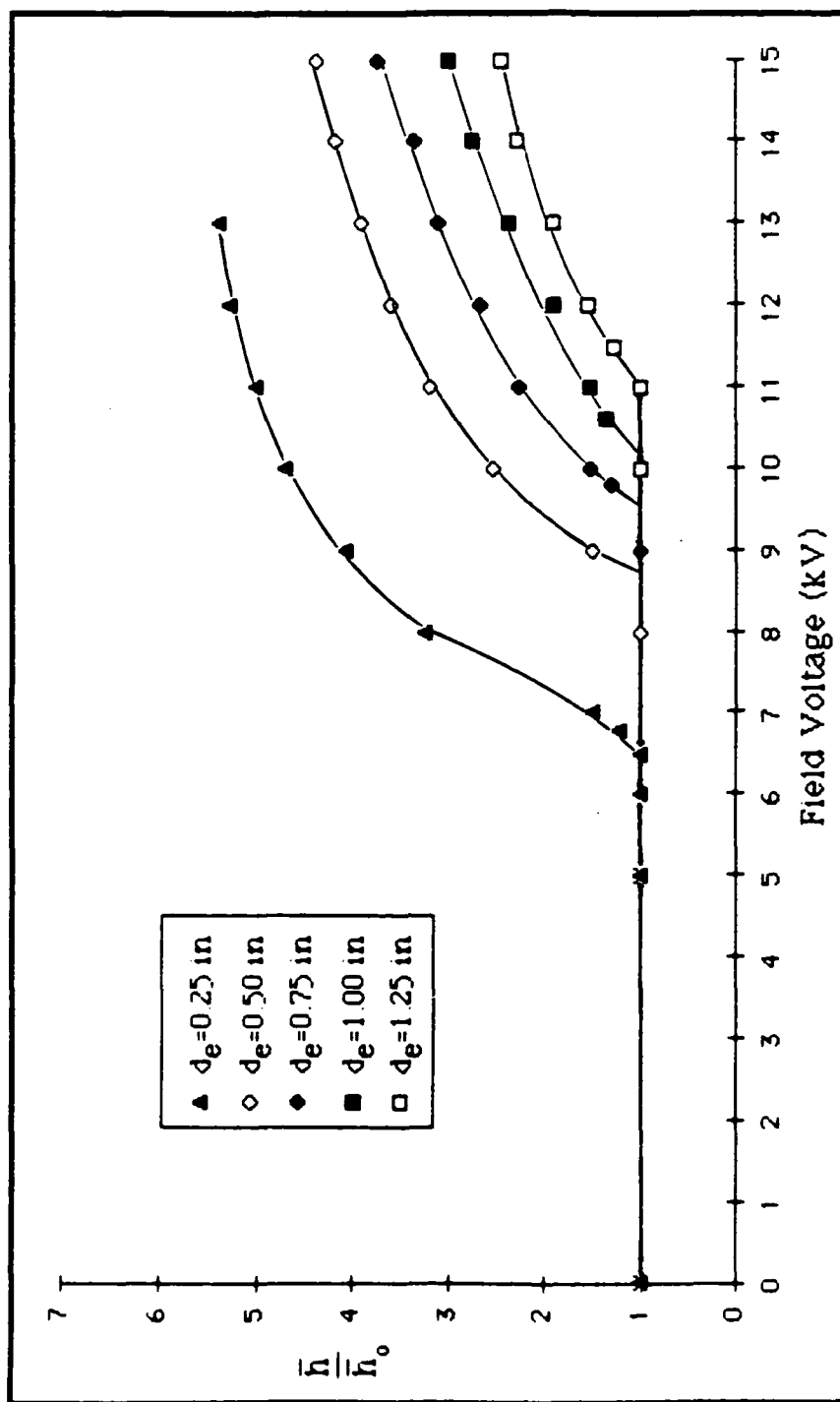
Emitter

Shroud

Nomenclature

Figure 13. Continued

Figure 14.   Effect of Field Voltage on the Ratio $\bar{h}/\bar{h}_0$ for the
0.0125 in diameter Stretched Wire Emitter at Various Emitter to
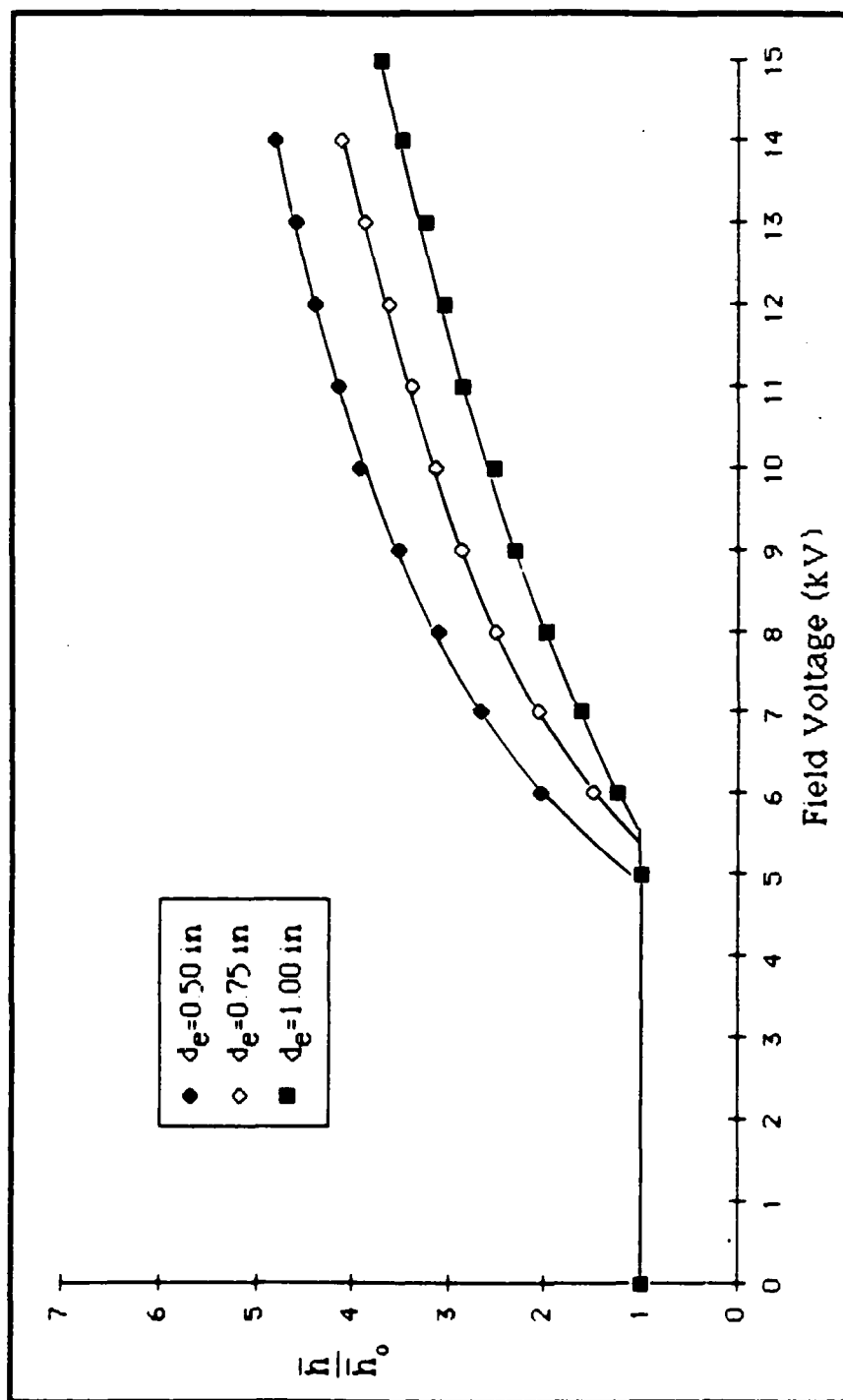Cylinder Distances, d_e

Figure 15. Effect of Field Voltage on the Ratio $\bar{h}/\bar{h}_o$ for the 0.004 in diameter Stretched Wire Emitter at Various Emitter to Cylinder Distances, d_e

Figure 16. Effect of Field Voltage on the Ratio $\bar{h}/\bar{h}_o$ for the Multipoint Emitter at Various Emitter to Cylinder Distances, d_e

Figure 17. Interferometer Photographs Showing the Effect of the Corona Wind on the Thermal Boundary Layer of the Cylinder Using the 0.004 in diameter Stretched Wire Emitter with $d_e = 0.5$ in

V=0
P=0

V=6 kV
P=0.078 watt

V=8 kV
P=0.512 watt

V=14 kV
P=6.482 watt

V=12 kV
P=3.516 watt

V=10 kV
P=1.66 watt

Figure 17. Continued

Figure 18. Effect of Field Power on the Ratio $\bar{h}/\bar{h}_o$ for the 0.004 in diameter Stretched Wire Emitter at Various Emitter to Cylinder Distances, d_e
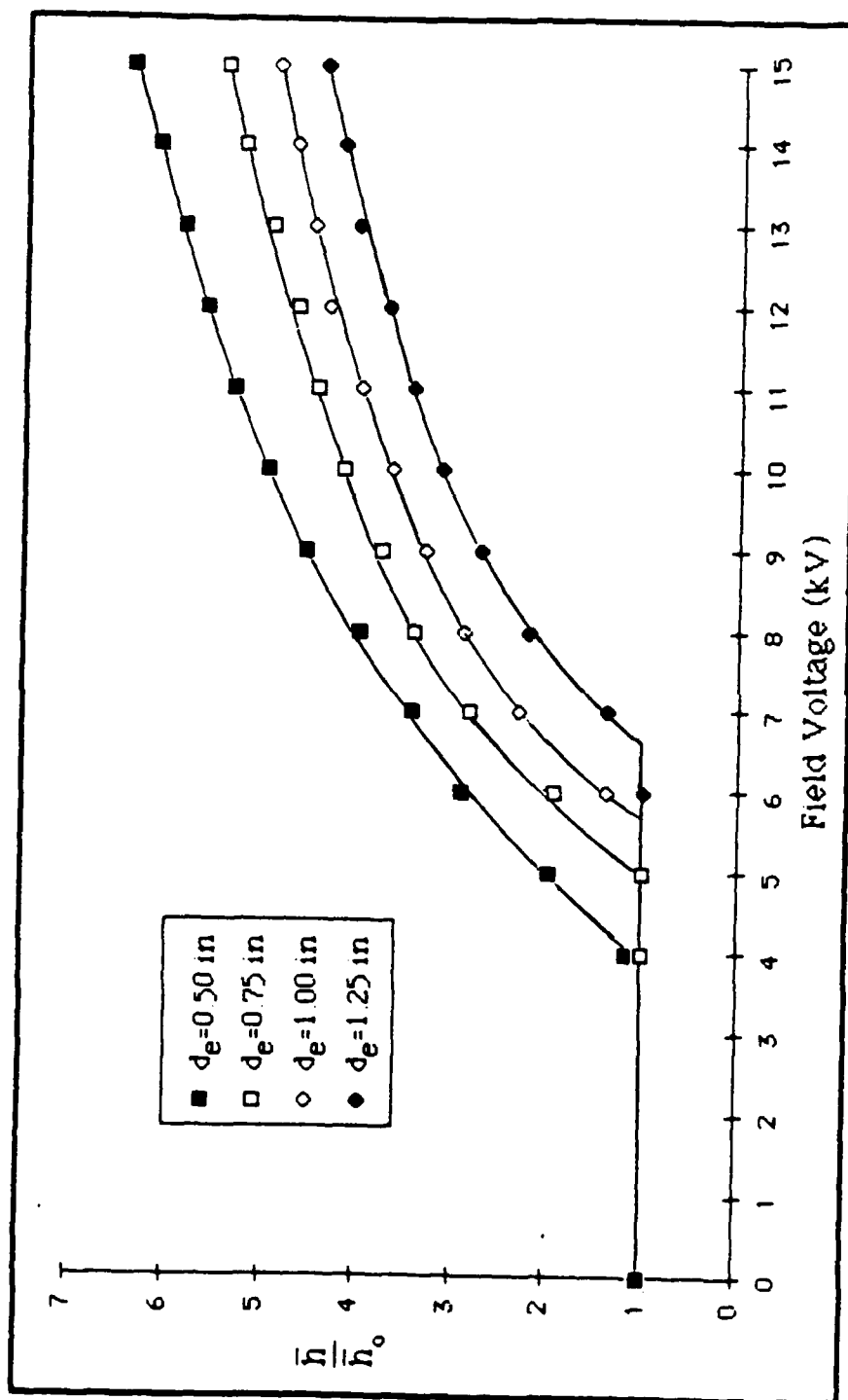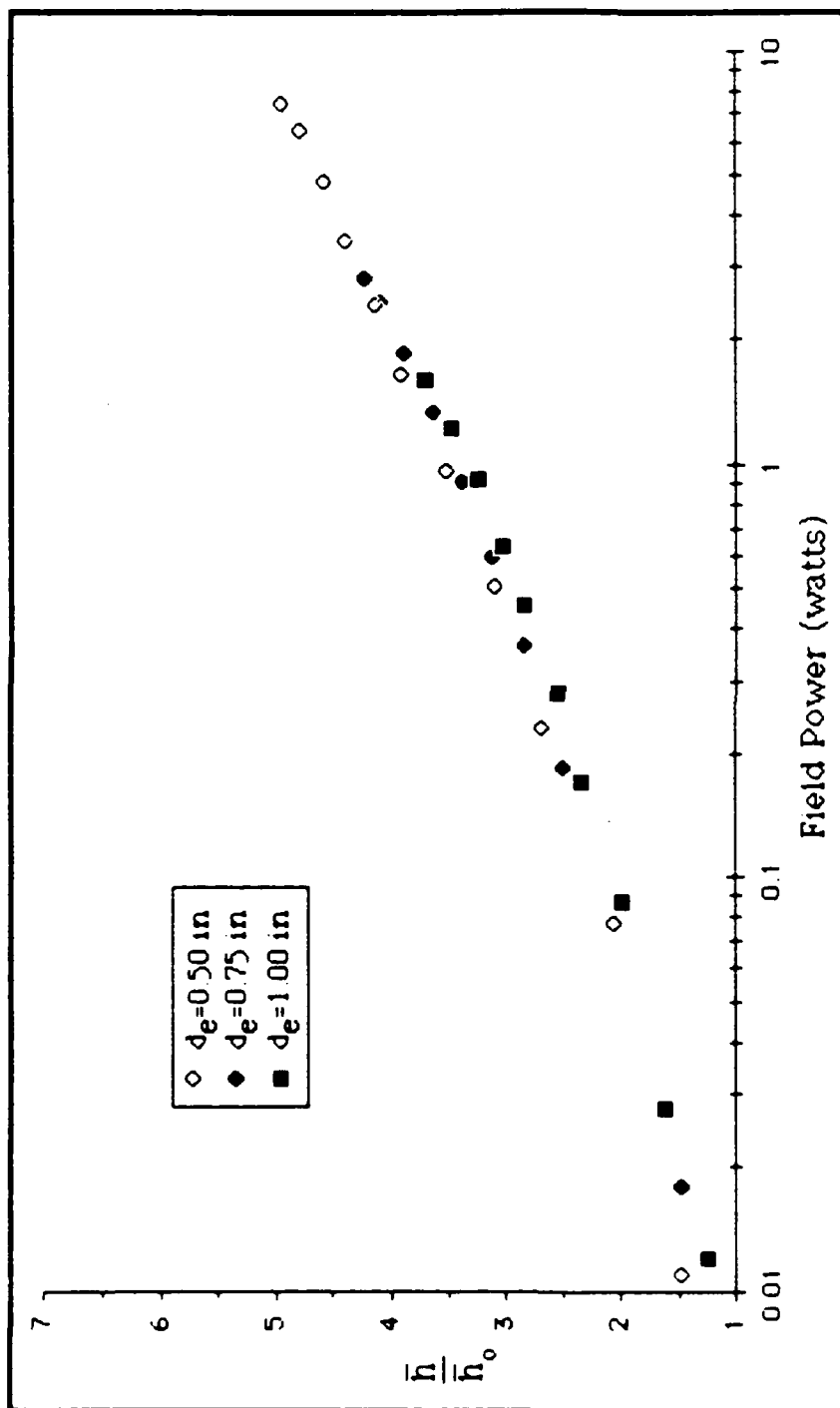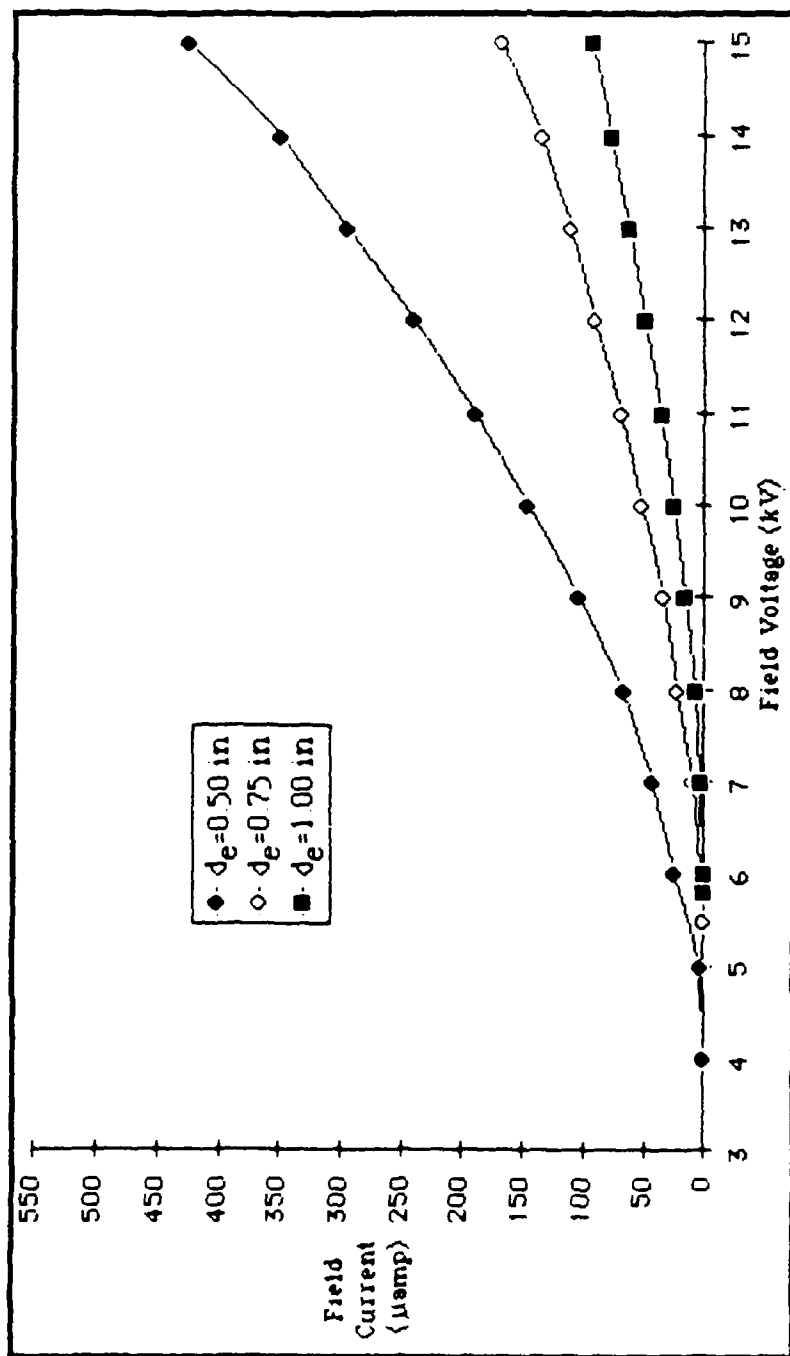
Figure 19. Relationship of Field Current to Field voltage for the 0.004 in diameter Stretched Wire Emitter at Various Emitter to Cylinder Distances, d_e

V=5 kV   V=6 kV   V=7 kV

P=0   P=0.009 watt   P=0.021 watt

Figure 20. Interferometer Photographs Showing the Effect of the Corona Wind on the Thermal Boundary Layer of the Cylinder Using the Multipoint Emitter with d_e =1.0 in
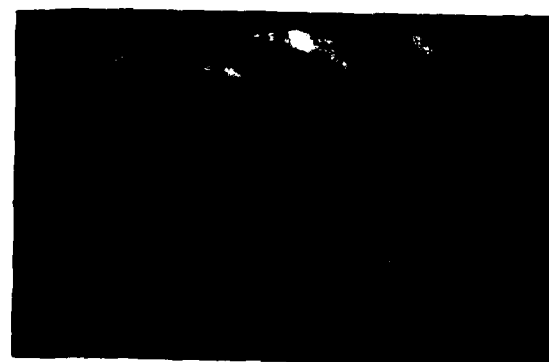
V=8 kV
P=0.064 watt

V=10 kV
P=0.260 watt

V=14 kV
P=1.078 watt

Figure 20. Continued
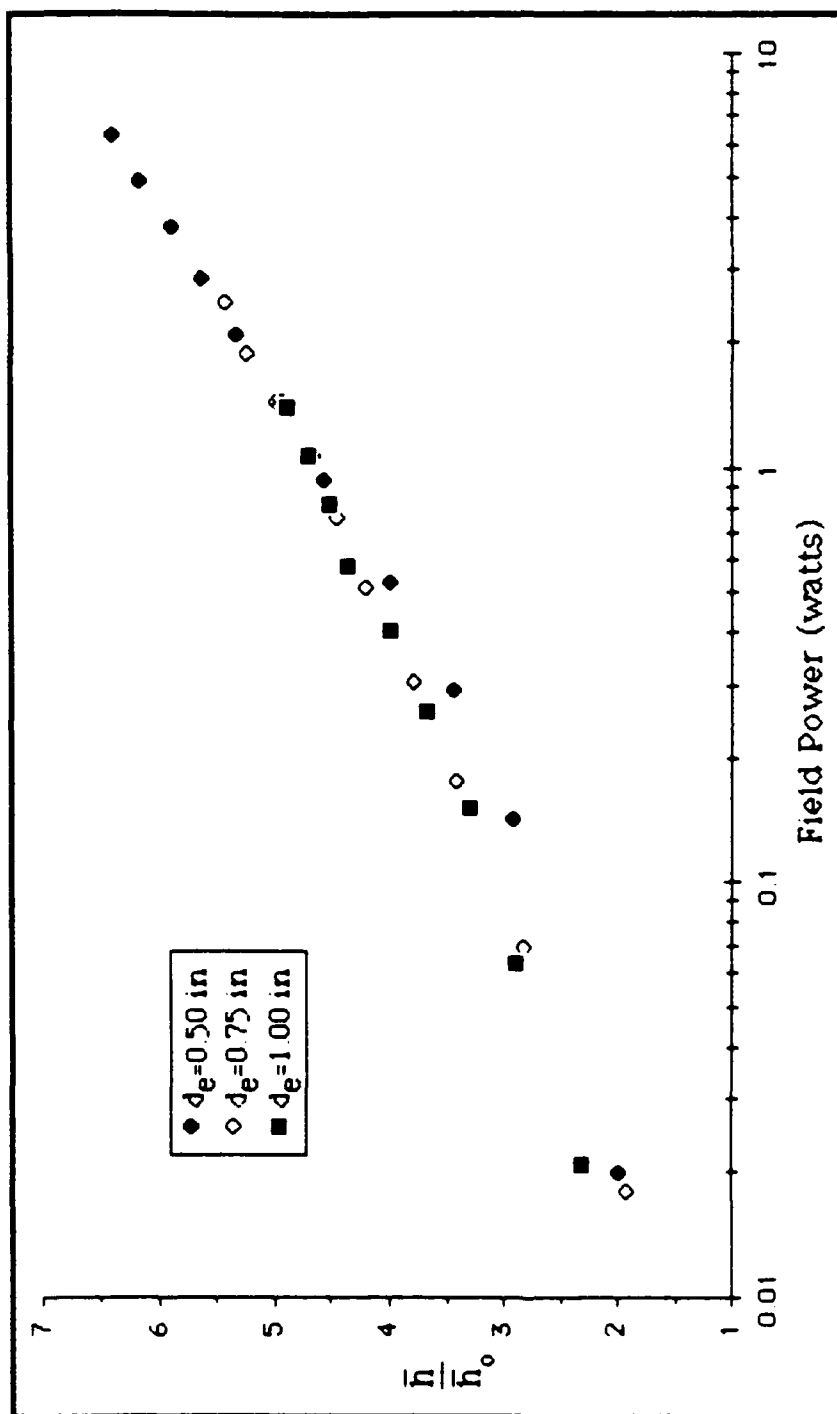
Figure 21. Effects of Field Power on the Ratio $\bar{h}/\bar{h}_o$ for the Multipoint Emitter at Various Emitter to Cylinder Distances, d_e
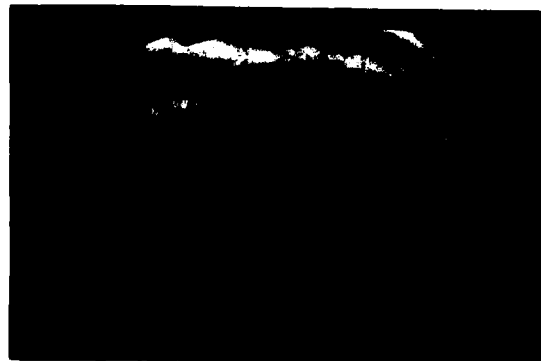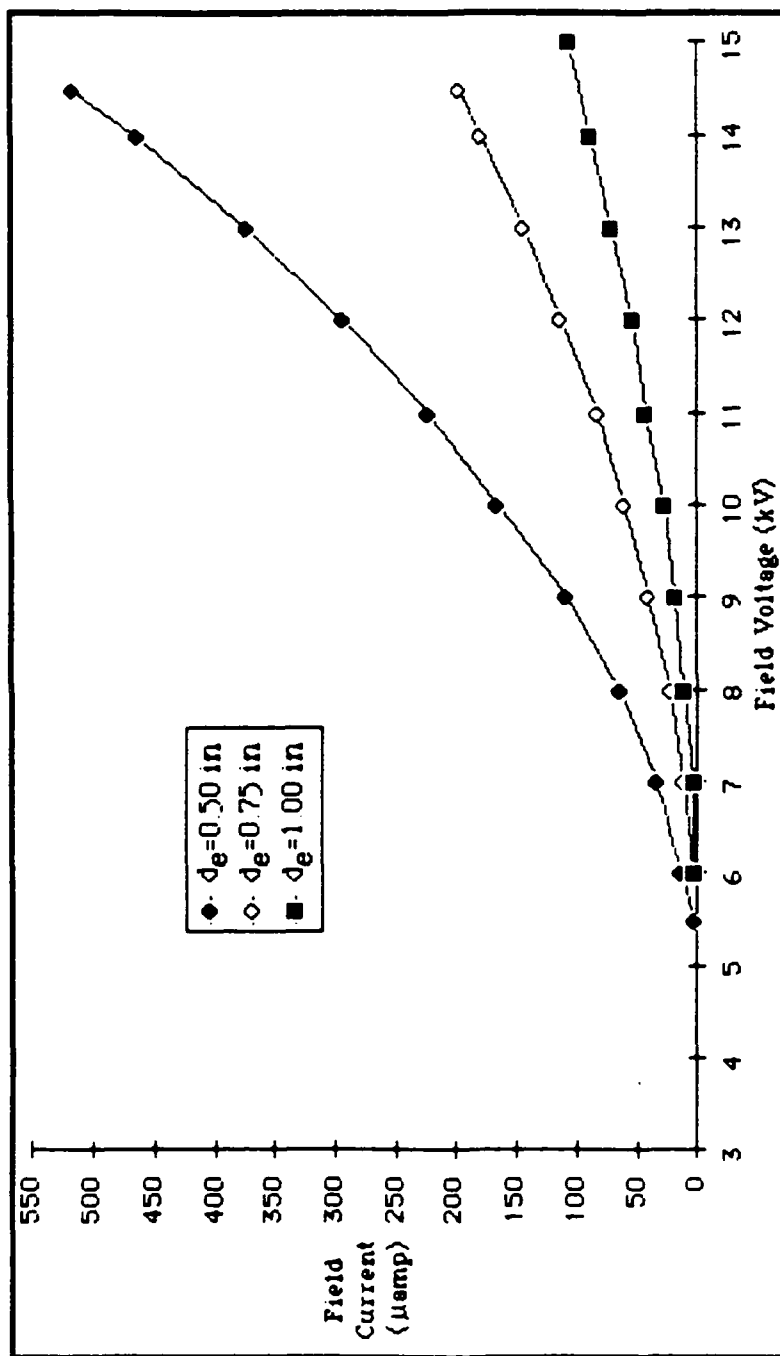
Figure 22. Relationship of Field Current to Field Voltage for the Multipoint Emitter at Various Emitter to Cylinder Distances, d_e
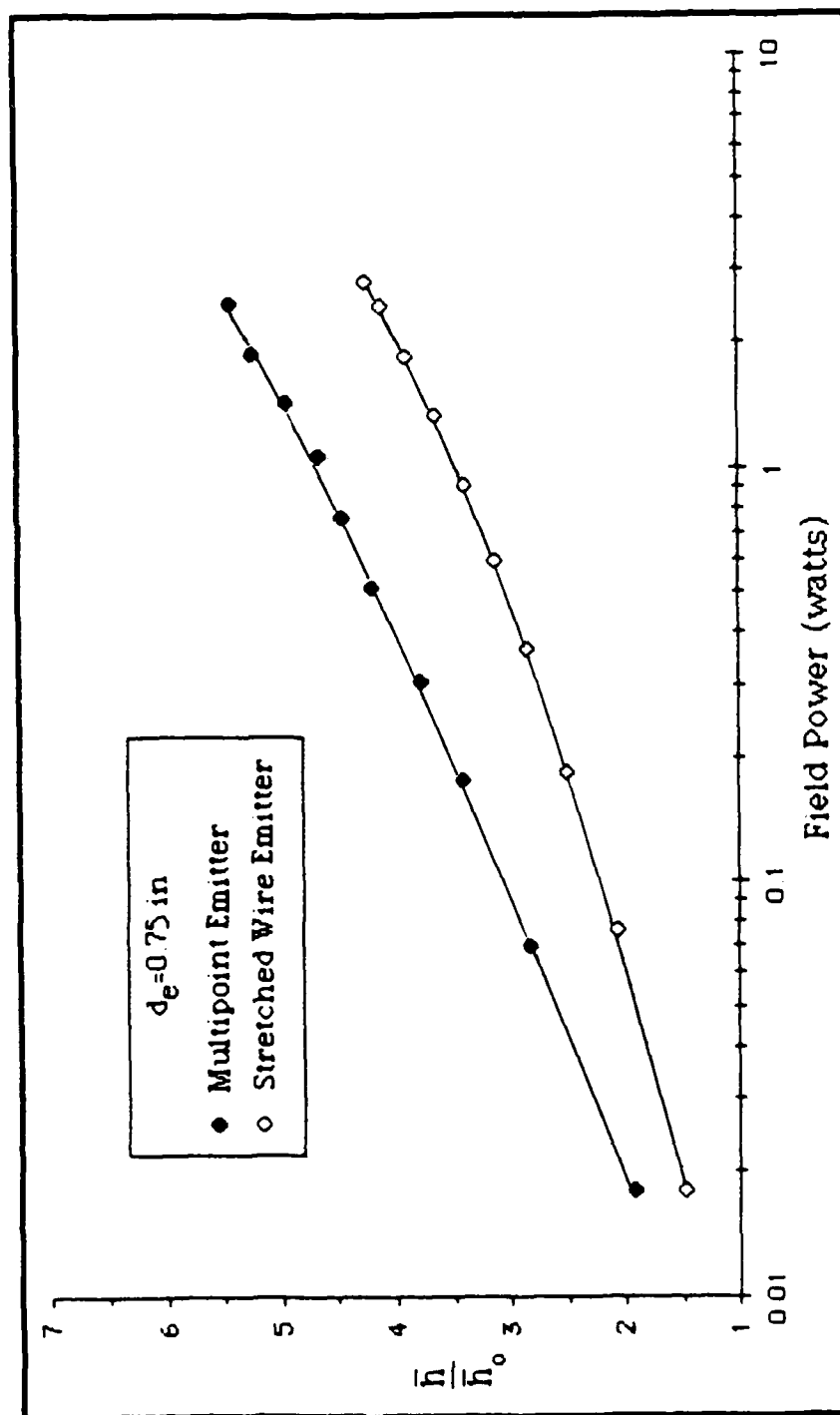
Figure 23. Comparison of the Effects of Field Power on $\bar{h}/\bar{h}_o$ for the 0.004 in diameter Stretched Wire Emitter and the Multipoint Emitter at the Same Emitter to Cylinder Distance, d_e = 0.75 in
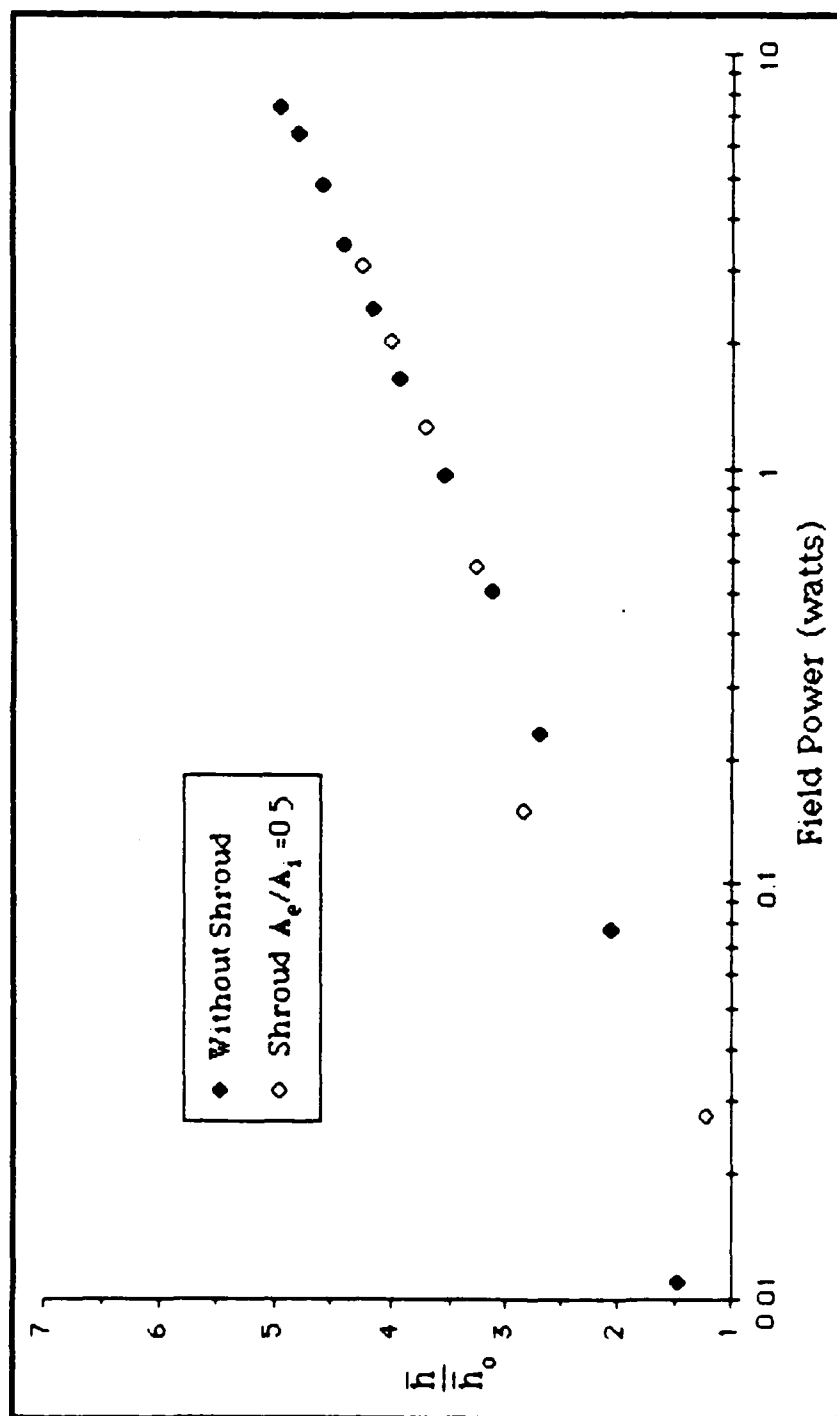
Figure 24. Comparison of the Effects of Field Power on $\bar{h}/\bar{h}_o$ for the 0.004 in diameter Stretched Wire Emitter with d_e = 0.5 in with and without Shroud
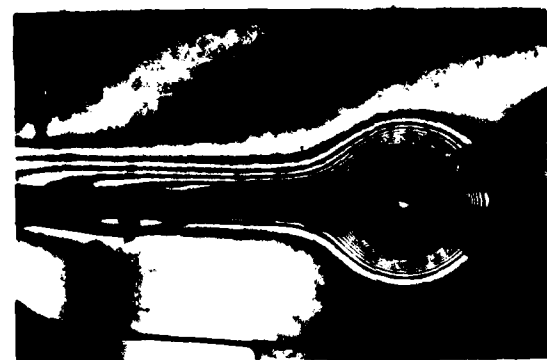
V=0
P=0

V=6 kV
P=0.12 watt

V=7 kV
P=0.511 watt

Figure 25.   Interferometer Photographs Showing the Effects of the
Corona Wind on the Thermal Boundary Layer of the Cylinder Using
the 0.004 in diameter Stretched Wire Emitter with d_e = 1.0 in,
d_m = 0.5 in, and Shroud A_e/A_i = 0.47

V=8 kV
P=1.072 watt

V=9 kV
P=1.917 watt

Figure 25. Continued

Figure 26. Effects of Field Power on $\bar{h}/\bar{h}_o$ for the 0.004 in diameter Stretched Wire Emitter with Four Configurations
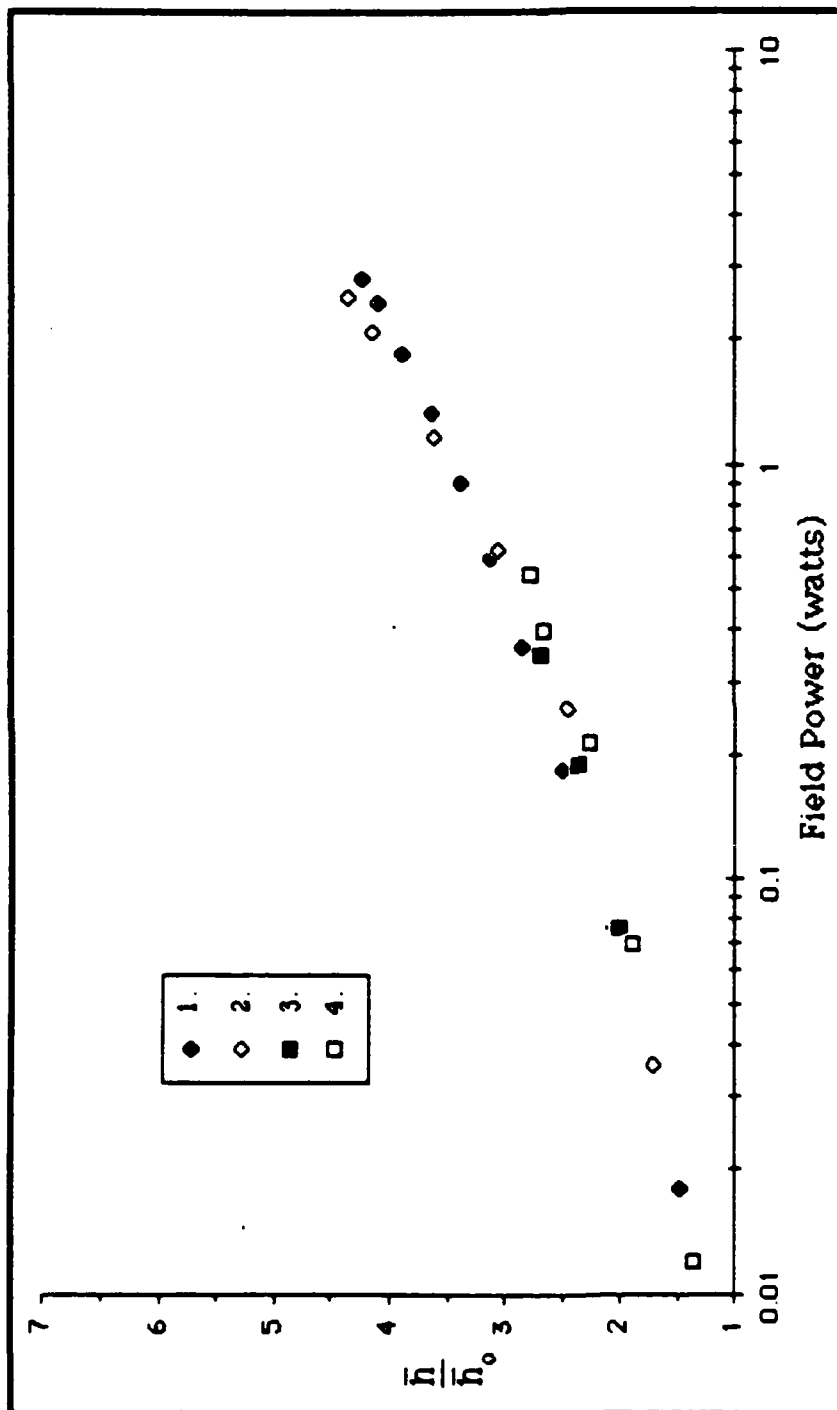
(1) d_e = 0.75 in, no grid, no shroud
(2) d_e = 1.0 in, d_m = 0.75 in, shroud A_e/A_1 = 0.47, d_s = 0.25 in
(3) d_e = 1.0 in, d_m = 0.75 in, shroud A_e/A_1 = 0.49, d_s = 0.75 in
(4) d_e ~ 0.78 in, d_m = 0.75 in, shroud A_e/A_1 = 0.49, d_s = 0.75 in

Figure 27. Effects of Field Power on $\bar{h}/\bar{h}_o$ for the Multipoint Emitter with Three Different Configurations
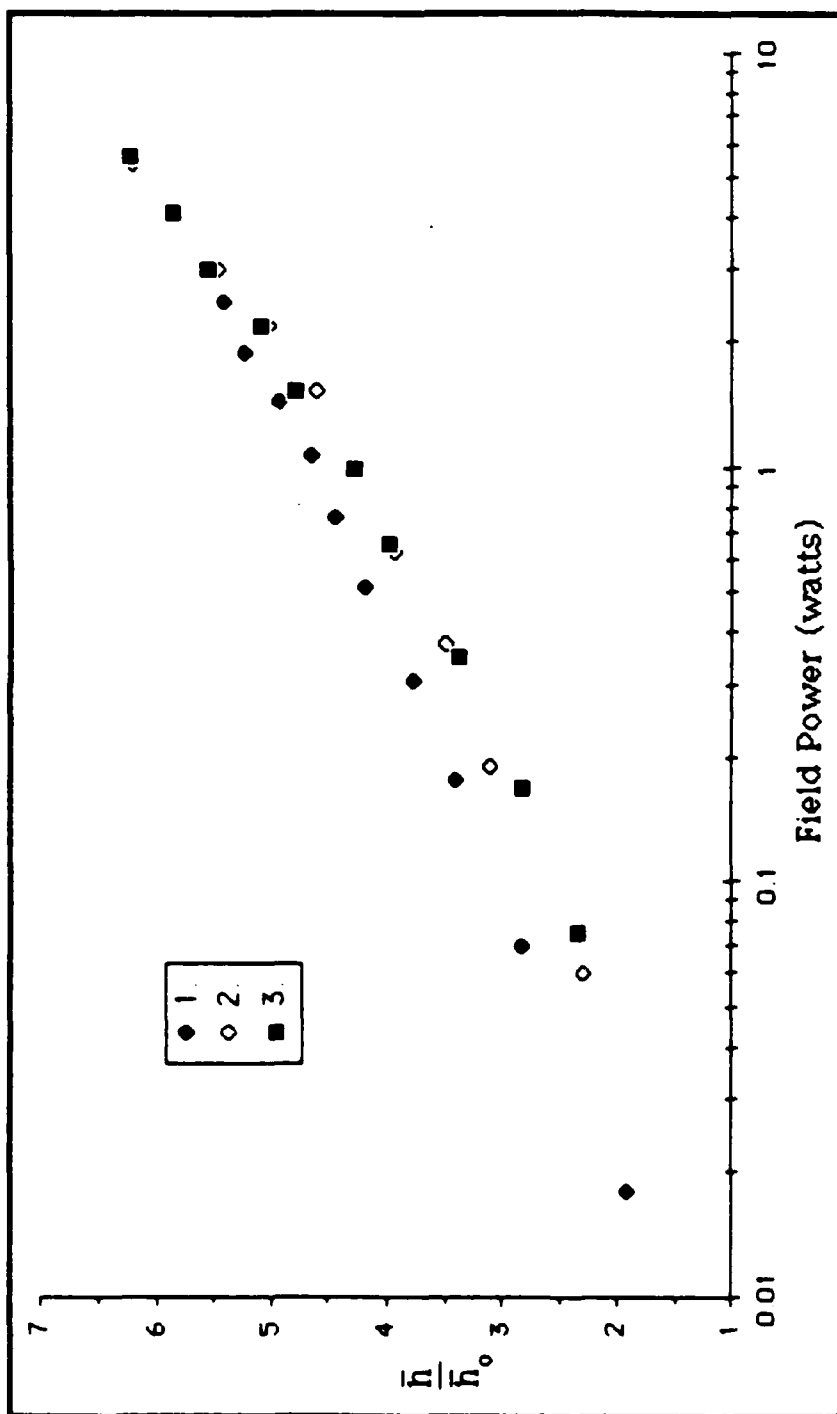
(1) d_e = 0.75 in, no grid, no shroud
(2) d_e ~ 0.78 in, d_m = 0.75 in, shroud A_e/A_1 = 0.49
(3) d_e = 1.0 in, d_m = 0.75 in, shroud A_e/A_1 = 0.49

64
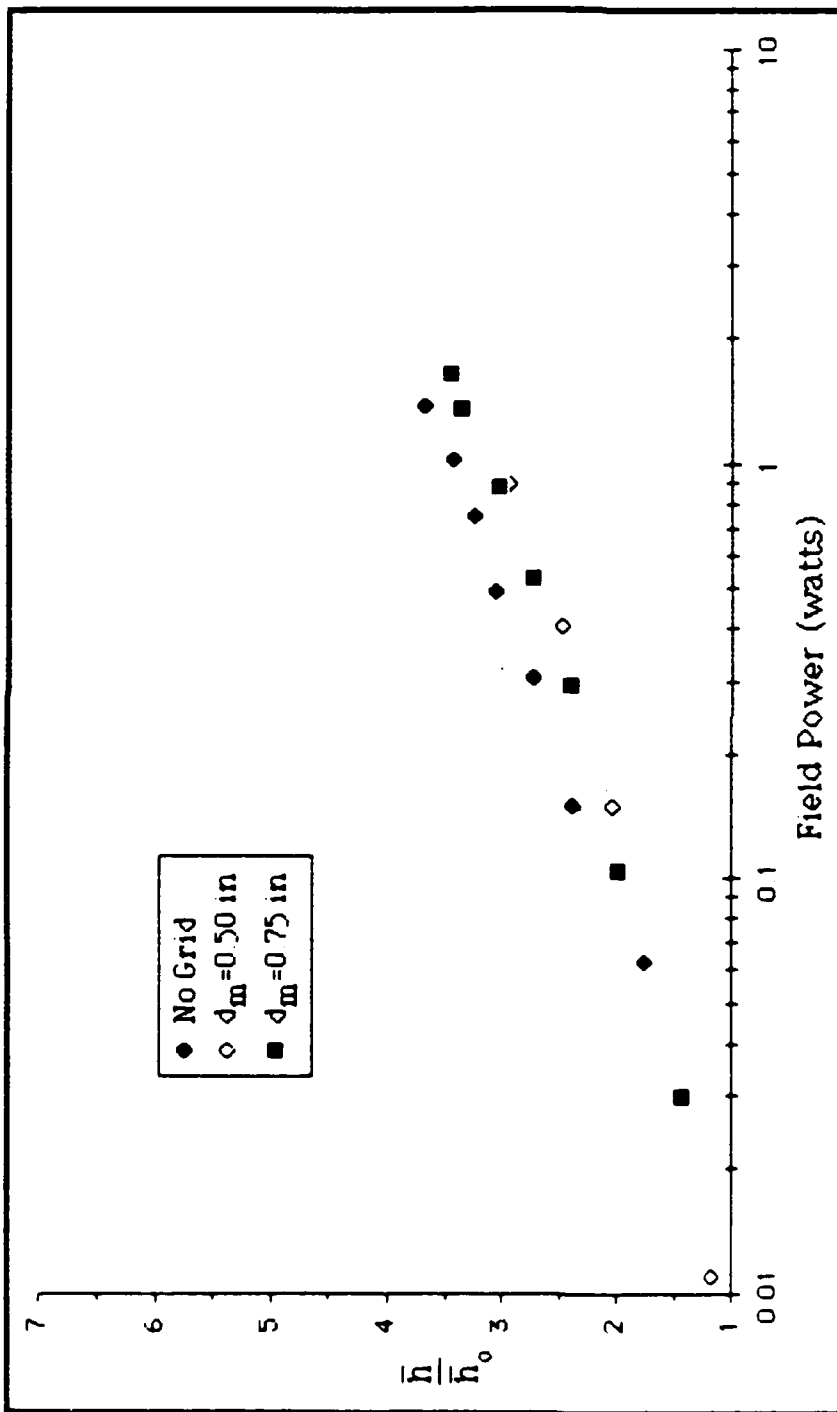
Figure 28. Effects of Field Power on $\bar{h}/\bar{h}_o$ for the 0.004 in diameter Stretched Wire Emitter with No Shroud, but Two Configurations with the Grid Compared to the Baseline with No Grid and No Shroud, $d_e = 1.0$ in
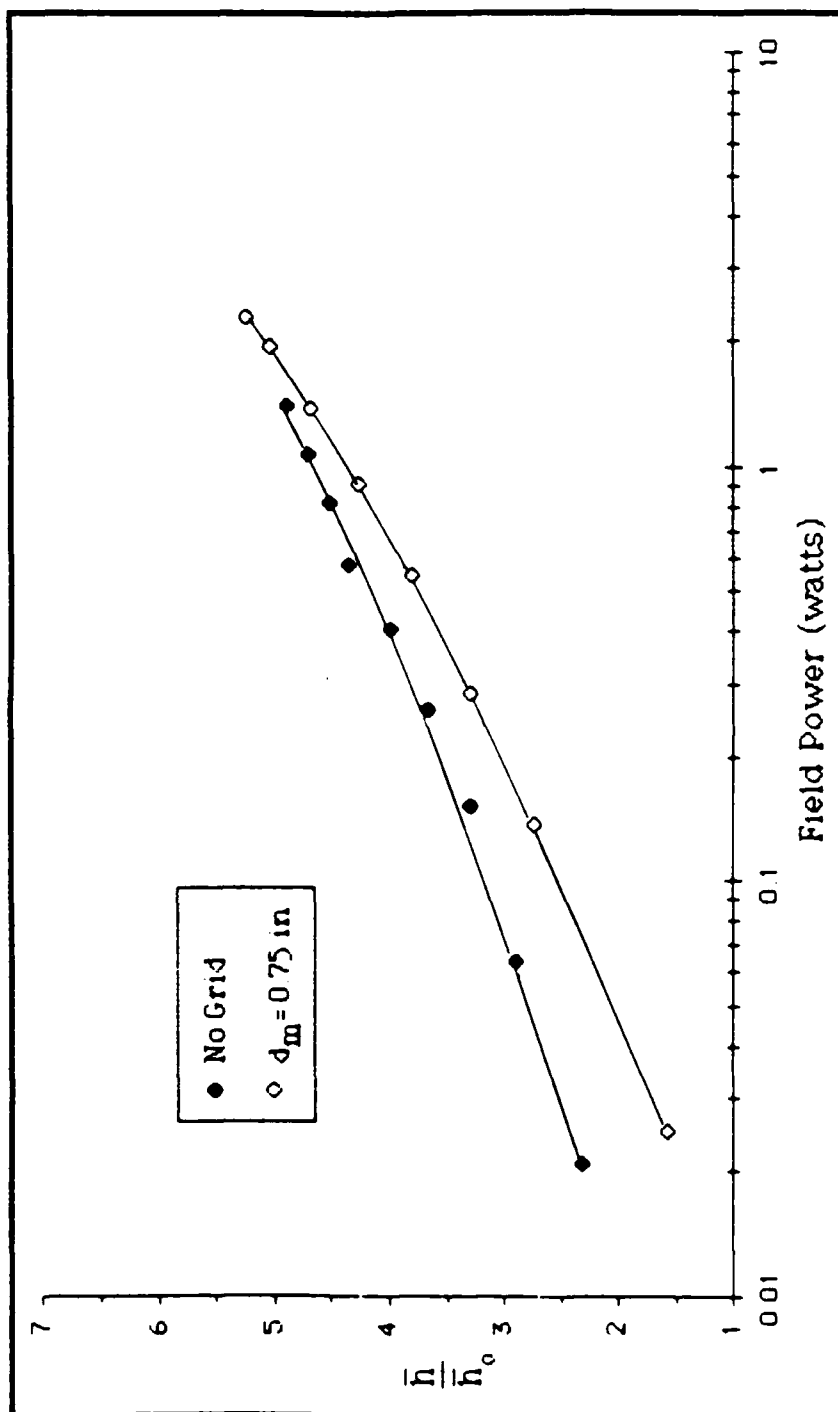
Figure 29. Effects of Field Power on $\bar{h}/\bar{h}_o$ for the Multipoint Emitter with No Shroud but a Configuration with the Grid Compared to a Configuration without the Grid, d_e = 1.0 in
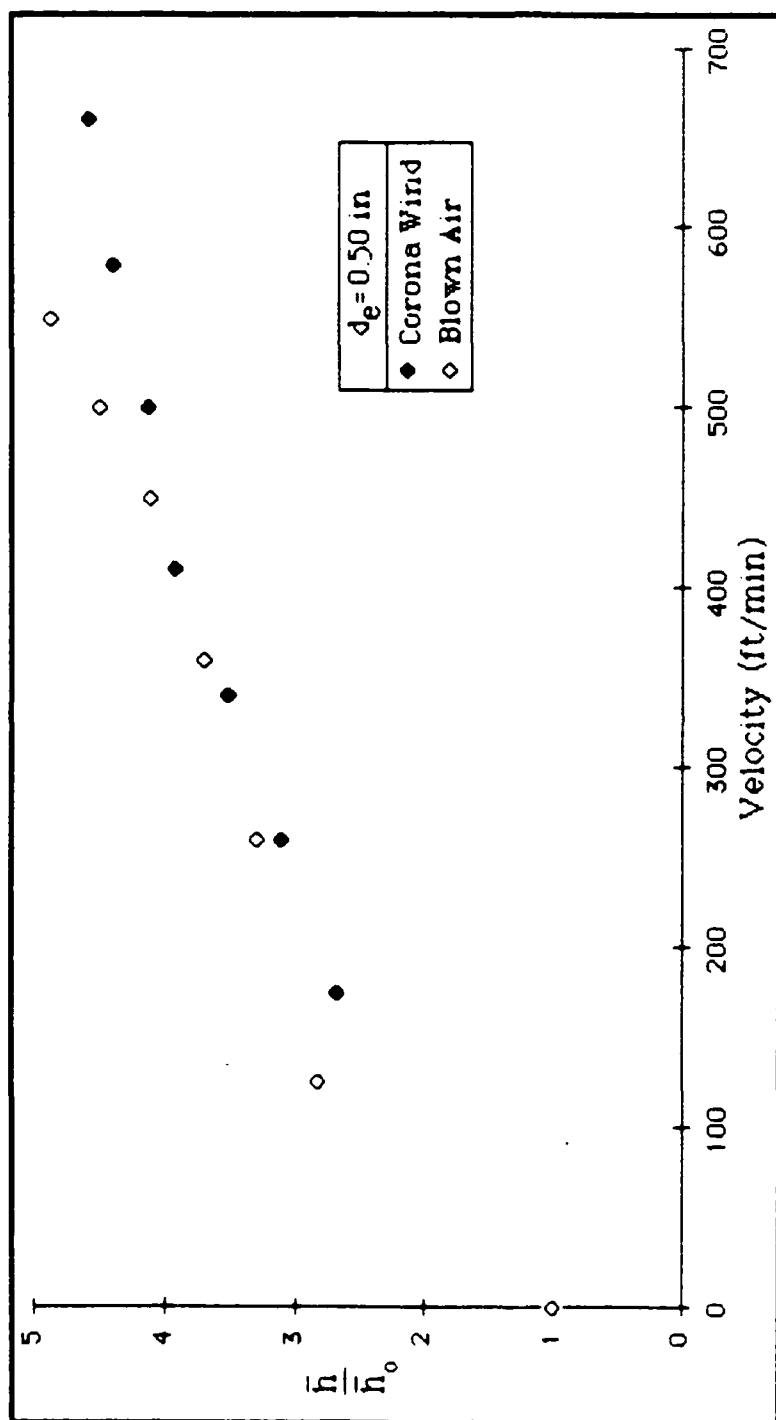
Figure 30. Effect of the Air Velocity on $\bar{h}/\bar{h}_o$ with $d_e = 0.5$ in for the Corona Wind (0.004 in Stretched Wire) and Uncharged Blown Air

67
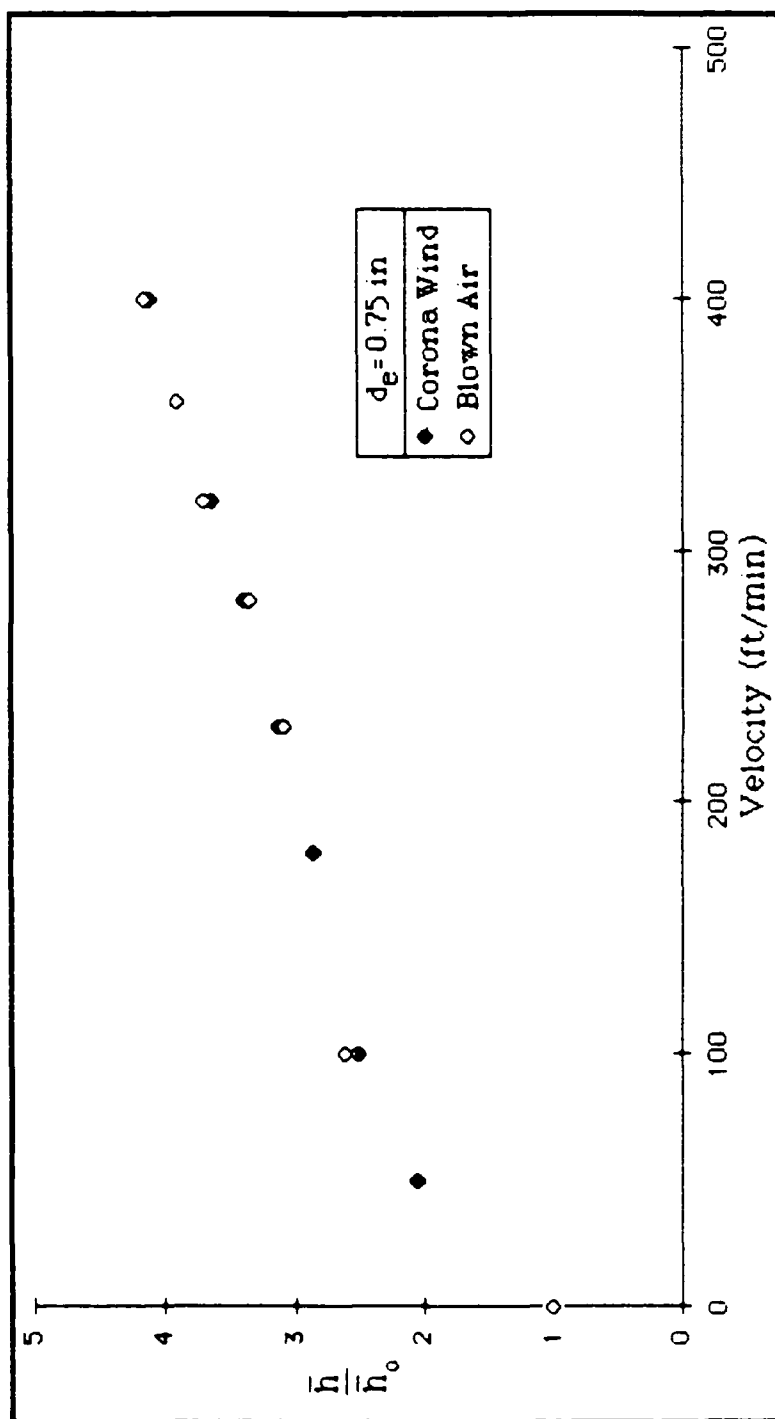
Figure 31. Effect of the Air Velocity on $\bar{h}/\bar{h}_o$ with d_e = 0.75 in for the Corona Wind (0.004 in Stretched Wire) and Uncharged Blown Air
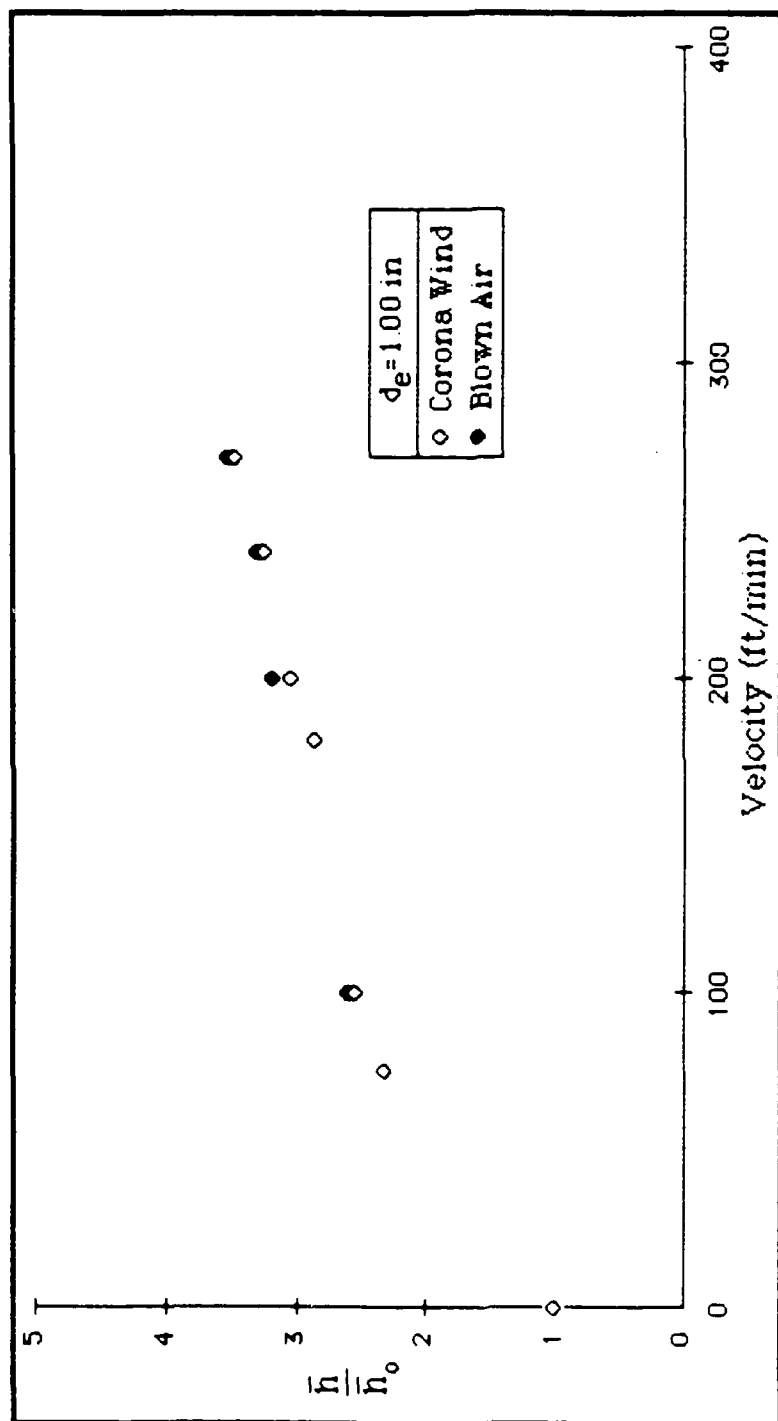
Figure 32. Effect of the Air Velocity on $\bar{h}/\bar{h}_o$ with $d_e = 1.0$ in for the Corona Wind (0.004 in Stretched wire) and Uncharged Blown Air
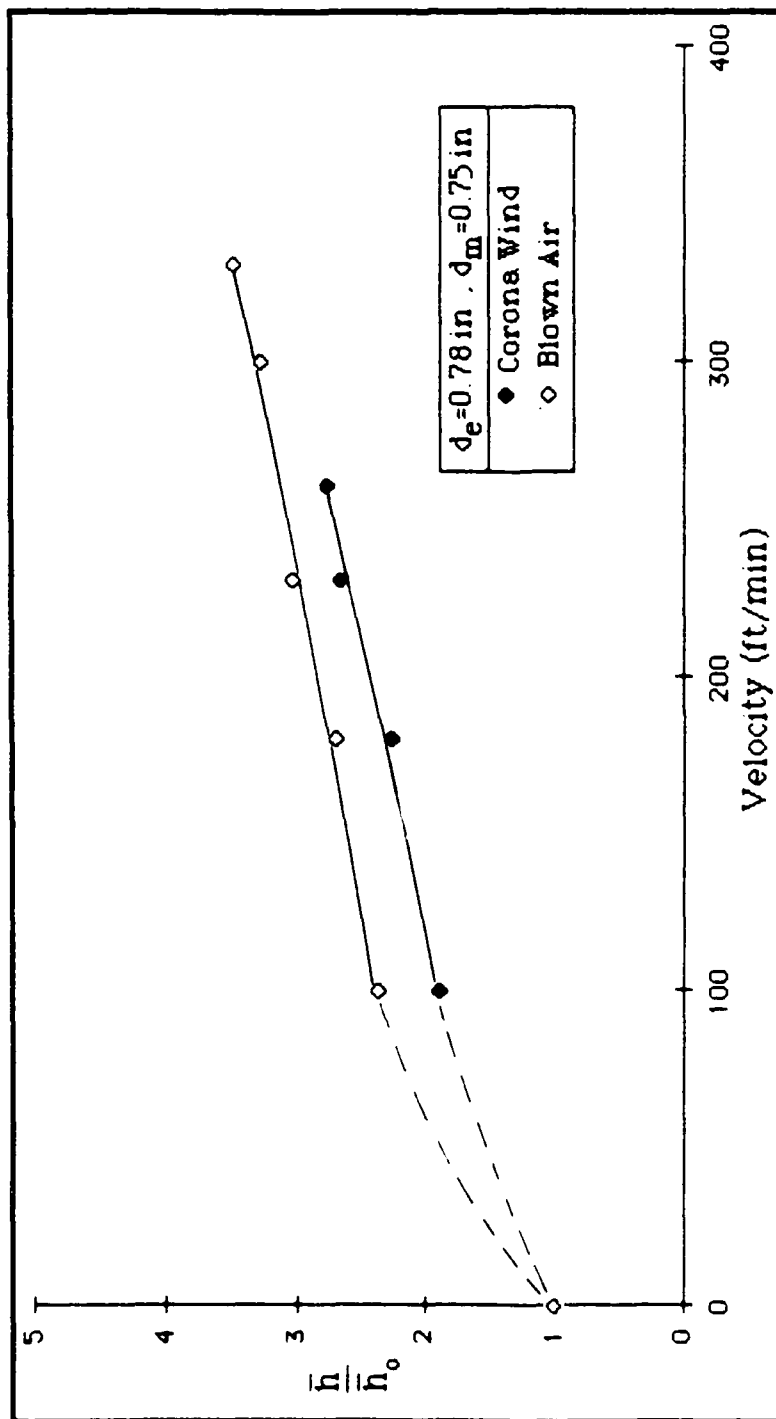
Figure 33. Effect of the Air Velocity on $\bar{h}/\bar{h}_o$ with the Grid Installed with $d_m = 0.5$ in and the Cylinder Approximately 1/32 in above the Grid to Give Approximate $d_e \sim 0.75$ in

APPENDIX A

Computer Listing of HP BASIC Program Used

in Thermocouple System

```
10   REM      THIS PROGRAM SCANS CHANNELS WITH COPPER-CONSTANTAN
20   REM      THERMOCOUPLES AND GIVES THE TEMPERATURE READING ON EACH
30   REM      CHANNEL IN BOTH DEGREES C AND F.  IT ALSO GIVES AVERAGE
40   REM      TEMPERATURE AND THE DELTA FROM AMBIENT
50   REM
60   REM
70   REAL REFJUNCT,TEMPF,TEMPC,VOLTAGE,AVGC,AVGF,AMBC,DELTC,DELTF
80   INTEGER X,Y,CHAN,COUNT
90   INPUT "ENTER RUN NUMBER", X
100  INPUT "ENTER DATE (DAY/MO)", Y
110  DATA 7,709,701
120  READ BUS,SCN,DVM
130  COM SCN,DVM,BUS
140  PRINTER IS 16
150  INPUT "ANOTHER PASS? (YES=1, NO=2) ", R
160  ON R GOTO 170,600
170  INPUT "FULL PRINTOUT? (YES=1, NO=2) ", S
180  ABORTIO BUS
190  REMOTE BUS
200  RESET BUS
210  OUTPUT DVM USING "K";"F1R7T2T3"
220  AVGC=0
230  AVGF=0
240  IMAGE /, "RUN NO.: ", DD, /,"DATE: ", DDDD,//
250  PRINT USING 240; X,Y
260  FOR CHANNEL=0 TO 13
270  REFJUNCT=0
280  OUTPUT SCN USING "F";VOLTAGE
290  TRIGGER DVM
300  ENTER DVM USING "F";VOLTAGE
310  TEMPC=FNTEMP(VOLTAGE,REFJUNCT)
320  TEMPF=TEMPC*1.8+32.0
330  REM
340  REM      HERE WANT TO CALCULATE THE AVERAGE CYLINDER TEMP USING A
350  REM      WEIGHTED AVERAGE WHERE THE CENTER OF THE CYLINDER IS GIVEN
360  REM      44% WEIGHTING AND THE ENDS ARE EACH GIVEN 28% WEIGHTING
370  REM
380  CHAN=CHANNEL+1
390  COUNT=CHANNEL DIV 4+1
400  ON COUNT GOTO 410,440,410,480
410  AVGC=AVGC+.07*TEMPC
420  AVGF=AVGF+.07*TEMPF
430  GOTO 510
440  AVGC=AVGC+.11*TEMPC
450  AVGF=AVGF+.11*TEMPF
460  GOTO 510
470  IMAGE "CHANNEL ", DD, ":",/, MDDD.D, "C", 2X, MDDD.D, "F", /
480  IF CHANNEL()13 THEN 520
490  AMBC=TEMPC
500  AMBF=TEMPF
510  ON S GOTO 520,530
520  PRINT USING 470;CHAN,TEMPC,TEMPF
```

```
530 NEXT CHANNEL
540 DELTC=AVGC-AMBC
550 DELTF=AVGF-AMBF
560 IMAGE "AVG CYL TEMP:", /, MDDD.D, "C", 2X, MDDD.D, "F", //, "DELTA
          TEMP", /, MDDD.D, "C", 2X, MDDD.D, "F", //
570 PRINT USING 560; AVGC,AVGF,DELTC,DELTF
580 OUTPUT DVM; "A1"
590 GOTO 150
600 END
610 DEFFNTEMP(VOLTAGE,RJUNCT)
620 COM SCN,DVM,BUS
630 DIM JUNCT(2),COEFF(8)
640 JUNCT(1)=3.6880238E1
650 JUNCT(2)=41277001E-2
660 COEFF(0)=.10086091
670 COEFF(1)=25727.94369
680 COEFF(2)=-767345.8295
690 COEFF(3)=78025595.81
700 COEFF(4)=-9247486589
710 COEFF(5)=6.97688E11
720 COEFF(6)=-2.66192E13
730 COEFF(7)=3.94078E14
740 COEFF(8)=1.00E13
750 TEMP=FNPOLY(COEFF(*),VOLTAGE+1E-6*((JUNCT(2)*RJUNCT+JUNCT(1))*
          RJUNCT))
760 RETURN TEMP
770 DEF FNPOLY(CO(*),VAL)=(((((((CO(8)*VAL+CO(7))*VAL+CO(6))*VAL+CO(5))
          *VAL+CO(4))*VAL+CO(3))*VAL+CO(2))*VAL+CO(1))*VAL+CO(0)
780 FNEND
```

Appendix B

Calculations for Predicted Free Convection Heat

Transfer Coefficient

An empirical model was used to calculate the predicted value of the free convection heat transfer coefficient. The following discussion repeats the equations on which the model is based and shows the calculation of $\bar{h}_o$ for the cylinder.

From the well-accepted empirical equation for a horizontal cylinder (1:364):

$$\overline{Nu} = 0.525 \left[(Gr)(Pr) \right]^{1/4} \tag{1}$$

where

$$\overline{Nu} = \bar{h}_o D/k \tag{2}$$

thus

$$\bar{h}_o = \frac{k(0.525) \left[(Gr)(Pr) \right]^{1/4}}{D} \tag{3}$$

For this system (1:361), with $T_w = 120$ F and $T_a = 70$ F:

$Pr = 0.706$, $Gr = 5.176 \times 10^4$

Then $\bar{h}_o = 1.358$ Btu/hr-ft^2-F

Considering that (1:363)

$$Q_{OC} = \bar{h}_o A \, \Delta T \tag{4}$$

then $Q_{OC} = 14.81$ Btu/hr $= 4.34$ watt

But this result is based on the approximation for a very long cylinder and does not include convective losses through the ends of the cylinder, so now a correction is needed.

Assume the ends of the cylinder are small vertical plates; then (1:367):

$$\bar{h}_{col} = 0.29 \left[\Delta T / D \right]^{1/4} \tag{5}$$

Then, for this system:

$$\bar{h}_{col} = 1.435 \text{ Btu/hr-ft}^2\text{-F}$$

Now, by using equation 4 applied to the cylinder ends:

$$Q_{col} = 0.782 \text{ Btu/hr} = 0.229 \text{ watt}$$

The radiative heat transfer rate can be calculated using the assumption that the cylinder is a small gray body and using the Planck function to find:

$$Q_r = \sigma \epsilon A (T_w^4 - T_a^4) \tag{6}$$

The value of the emissivity, ϵ, for polished 2024 aluminum is 0.07, thus, for the cylinder

$$Q_r = 0.94 \text{ Btu/hr} = 0.275 \text{ watt}$$

Upon examination of equation (6), it can be seen that if the ambient temperature is held constant and the cylinder temperature is held relatively constant, say $\pm$ 5 R, then the radiative heat transfer can be assumed to be constant. This assumption is further reinforced by noting that Q_r is an order of magnitude smaller than Q_{oc}.

Now, if we neglect conductive heat losses from the cylinder, then the total heat transfer rate is:

$$Q_t = Q_{oc} + Q_{col} + Q_r \tag{7}$$

and subsituting in gives

$$Q_t = 16.53 \text{ Btu/hr} = 4.84 \text{ watt}$$

APPENDIX C

Computer Listing of BASIC Computer Program Used

for Interferometer Data

```
10  REM      HOGUE (GA-84D) INTERFEROMETER DATA PROGRAM
20  REM      L=RUN NUMBER
30  REM      XACT=ACTUAL LENGTH OF REFERENCE WIRE, INCHES
40  REM      XSCAL=MEASURED LENGTH OF REFERENCE WIRE IN PHOTO, INCHES
50  REM      CM=MOLECULAR WEIGHT OF AIR, LBM/LB MOLE
60  REM      NN=TOTAL NUMBER OF STATIONS MEASURED, USUALLY 7
70  REM      KK=TOTAL NUMBER OF FRINGES
80  REM      TC=TEST SECTION TEMPERATURE, R
90  REM      PC=TEST SECTION PRESSURE, IN OF HG
100 REM
110 DIM SD1(10),SD2(10),SD3(10),X1(10),X2(10),X3(10),Y1(10),Y2(10),Y3
 (10),H(10),TW(10),R(10),T(10),WALL1(10),WALL2(10),F1(10),F2(10),F3(10)
120 INPUT L,XACT,XSCAL,CM,NN,KK,TC,PC
130 C=XACT/XSCAL
140 S=KK
150 A=(70.73*CM*PC)/1545.4
160 RC=A/TC
170 LPRINT "POS'N I      H        TW        TF1        TF2        TF3":LPRINT
180 FOR I=1 TO NN
190 INPUT "NEXT WALL(X,Y),F1(X,Y),F2(X,Y),F3(X,Y)",WALL1(I),WALL2(I),
 X1(I),Y1(I),X2(I),Y2(I),X3(I),Y3(I)
200 Y1(I)=Y1(I)*2.54:Y2(I)=Y2(I)*2.54:Y3(I)=Y3(I)*2.54  'CONVERT TO CM
210 F1(I)=SQR((X1(I)-WALL1(I))^2+(Y1(I)-WALL2(I))^2)
220 F2(I)=SQR((X2(I)-WALL1(I))^2+(Y2(I)-WALL2(I))^2)
230 F3(I)=SQR((X3(I)-WALL1(I))^2+(Y3(I)-WALL2(I))^2)
240 SD1(I)=ABS(F1(I)*.393701)
250 SD2(I)=ABS(F2(I)*.393701)
260 SD3(I)=ABS(F3(I)*.393701)
270 F1(I)=C*SD1(I):F2(I)=C*SD2(I):F3(I)=C*SD3(I)
280 NEXT I
290 R(KK-2)=RC-(.000589*(S-2.5))
300 R(KK-1)=RC-(.000589*(S-1.5))
310 R(KK)=RC-(.000589*(S-.5))
320 T(KK-2)=A/R(KK-2)
330 T(KK-1)=A/R(KK-1)
340 T(KK)=A/R(KK)
350 DELT1=T(KK)-T(KK-1)
360 DELT2=T(KK-1)-T(KK-2)
370 CK=.01516+(T(KK)-540)*.0067/270
380 HA=0
390 FOR I=1 TO NN
400 GRAD1=DELT1/(F2(I)-F1(I))
410 GRAD2=DELT2/(F3(I)-F2(I))
420 AV=.5*(GRAD1+GRAD2)
430 TW(I)=T(KK)+AV*F1(I)
440 H(I)=(12*CK*AV)/(TW(I)-TC)
450 HA=HA+H(I)
460 LPRINT USING "    ##    ";I;
470 LPRINT USING "   #.###";H(I);
480 LPRINT USING "     ###.#";TW(I);T(KK);T(KK-1);T(KK-2):LPRINT
490 NEXT I
500 HAV=HA/NN
510 LPRINT:LPRINT "AVERAGE HEAT TRANSFER COEFFICIENT = ";HAV
520 END
```

POS'N I		TW	TF1	TF2	TF3
1	1.185	576.3	573.5	568.5	563.7
2	1.479	577.1	573.5	568.6	563.7
3	1.752	576.1	573.5	568.6	563.7
4	1.862	575.2	573.5	568.6	563.7
5	1.312	578.5	573.5	568.6	563.7
6	1.339	577.6	573.5	568.6	563.7
7	1.143	578.4	573.5	568.6	563.7

AVERAGE HEAT TRANSFER COEFFICIENT = 1.43878

Figure 34. Typical Results from Computer Used to Reduce Interferometer Data
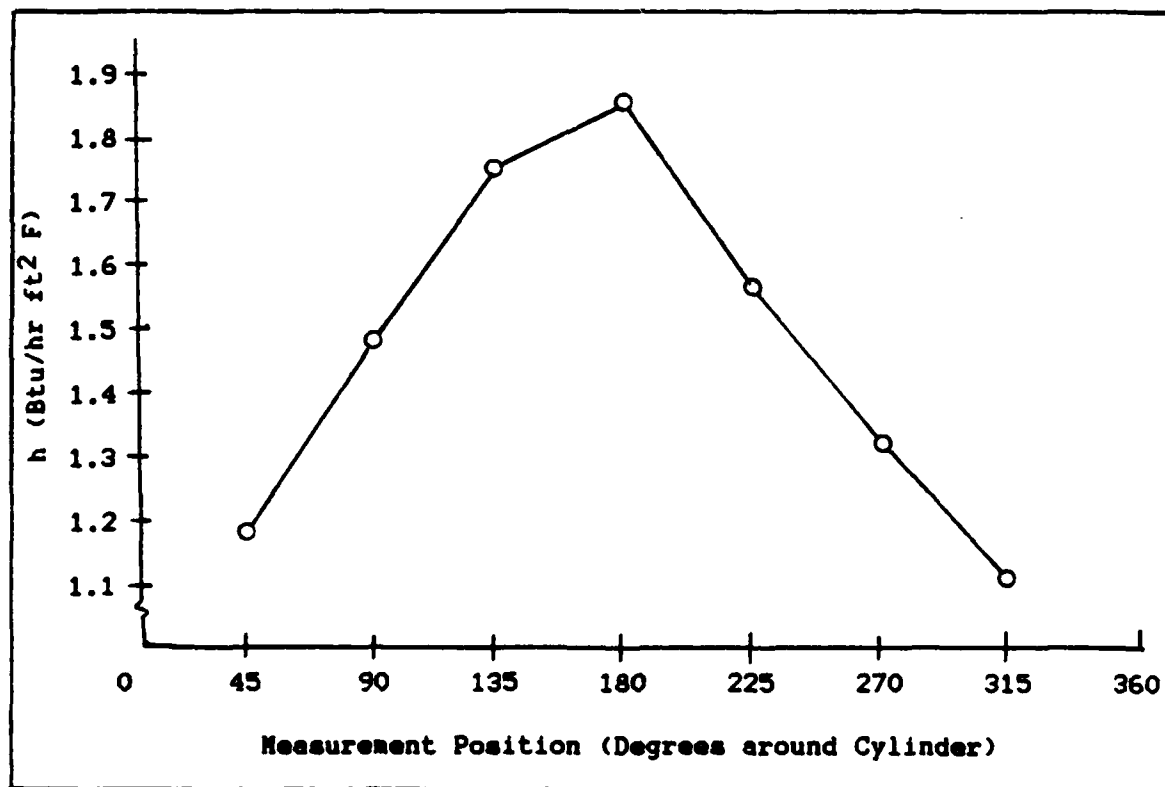
Figure 35. Variation of Local Convective Heat Transfer Coefficient Around Surface of Cylinder for Free Convection

78

Appendix D

Equipment List and Specifications

The experimental equipment used in this study is listed here. Each entry is in the following format: name, manufacturer, model or type number, serial number (SN), and range.

Interferometer and Camera System

1. Interferometer, Gaertner Scientific Corp., 8 inch optics

2. Light Source, General Electric Co., Magda Sunlight Lamp Type S-4, 100 watt

3. Mirror, concave, 45 inch focal length, 7.5 inch diameter

4. Polaroid Camera, Graflex, with Polaroid Type 42 film

Thermocouple System

1. System Controller, Hewlett-Packard, 9835B with Real Time Clock and HP-IB interface options, SN 1637A01722

2. Digital Voltmeter, Hewlett-Packard, 3455A, SN 1622A09252 Auto-scaled 0-0.1 volts

3. Scanner, Hewlett-Packard, 3495A, SN 1428A05735, 20 channel

4. Printer, Facit Corp., Model 4555, SN 8180050

5. Thermocouple Wire, Type T (Copper and Constantan), 30 gage, teflon wrapped

6. Dewar Flask (for Ice Bath)

Low Voltage AC System

1. Digital Multimeter, Hewlett-Packard, 3466A, SN 1716A18855, 0-2 ma (RMS) scale

2. Variable Auto Transformer, Standard Electrial Products Co., Type 500B, SN A3929, 0-135 volts AC

3. Nichrome Alloy Heater Element Wire, Driver-Harris, 0.0125 in diameter

High Voltage DC System

1. High Voltage DC Power Supply, NJE Corp., Model H-30-35, SN 11806, 0-30 kV, 0-35 ma

2. Electrostatic Voltmeter, Sensitive Research Instrument Corp., Model ESH, SN 102132, 0-15 kV

3. DC Microammeter, Hickok Electrical Instrument Co., Model 14, 0-50 μa, 0-100 μa, 0-200 μa, 0-500 μa

4. DC Microammeter, Westinghouse Electric Corp., Style 1164269, 0-200 μa

5. DC Microammeter, Simpson Electric Co., Model 26, 0-100 μa

6. DC Microammeter, Burlington Instrument Co., Model 331, 0-200 μa

7. DC Microammeter, Simpson Electric Co., Model 26, 0-20 μa

8. DC Microammeter, Simpson Electric Co., Model 26, 0-500 μa

Blown Air System

1. Dual Power Supply, Hewlett-Packard, 6205B, SN 07980, 0-40 VDC

2. Pressure Transducer, Bell and Howell Corp., SN 9510, 0-25 psig

3. High Pressure Compressed Air Hose, 1/2 in

Miscellaneous Equipment

1. Velometer, Alnor Instrument Co., Model 6000AP, SN 6077AA

2. Traversing Microscope, Central Scientific Co., SN 78039-2279

3. Thermometer, Fisher Scientific, Type 14-983-15B, 0-230 F

4. Sling Psychrometer, Taylor Instrument Co.

5. Calipers, Lufkin, Type 701, 0-6 in, 1/1000 in calibration

BIBLIOGRAPHY

1. Chapman, Alan J. Heat Transfer (Second Edition). New York: The Macmillan Company, 1967.

2. Demorest, K. E. and Gause, R. L. "Parameters Affecting Electrostatic Cooling," Internal Note IN-EH 11-74-2, Engineering Physics Div., Materials and Processes Lab., NASA/Marshall Space Flight Center, MSFC, AL 9 Sep 1974.

3. Eckert, Ernst R. G. and Goldstein, Richard J. Measurements in Heat Transfer (Second Edition). Washington, D. C.: Hemisphere Publishing Company, 1976.

4. Franke, M. E. "Effect of Vortices Induced by Corona Discharge on Free Convection Heat Transfer from a Vertical Plate," ASME Journal of Heat Transfer, 89: 427-433 (August 1969)

5. Franke, M. E. Effects of Electrostatic Fields on Free Convection Heat Transfer from Plates in Air. PhD Dissertation. The Ohio State University, Columbus, OH, 1967

6. Ho, Stephen S. Effects of Electrostatic Fields on Heat Transfer Under Forced Convection Conditions. MS Thesis, GAM/ME/69-7, School of Engineering, Air Force Institute of Technology (AU), WPAFB, OH, 34, March 1969.

7. Mitchell, A. S. and Williams, L. E. "Investigation of Heat Transfer by Corona Wind from a Horizontal Surface" Final Report prepared for Naval Air Systems Command (AIR-52022) Arlington, VA, December 1976 (AD-B017224L)

8. O'Brien, R. J. and Shine, A. J. "Some Effects of an Electric Field on Heat Transfer from a Vertical Plate in Free Convection," ASME Journal of Heat Transfer 89: 114-116 (Feb 1967)

9. O'Brien, R. J. The Effect of an Electric Field on Heat Transfer from a Vertical Plate in Various Gases Over a Range of Pressures. MS Thesis, GA/ME/64-3, School of Engineering, Air Force Insitute of Technology (AU), WPAFB, OH, 44-49, August 1964

10. Reynolds, B. L. and Holmes, R. E. "Heat Transfer in a Corona Discharge," Mechanical Engineering, 44-49 (October 1976)

82

11. Shannon, R. L. and Pogson, J. T. "Heat Transfer Augmentation Using a Corona Discharge Jet," ASME Paper 78-ENAs-8, Intersociety Conference on Environmental Systems, San Diego, CA, July 1978

12. Stefkovich, M. E. Effects of Nozzle and Grid Acceleration of Corona Wind on Cooling of a Vertical Flat Plate. MS Thesis, GAE/AA/83D, School of Engineering, Air Force Institute of Technology (AU), WPAFB, OH, December 1983.

13. Velkoff, H. R. and Kulacki, F. A. "Electrostatic Cooling," ASME Paper 77-DE-36, ASME Design Engineering Conference and Show, Chicago, IL, May 1977

14. Velkoff, H. R. and Marco, S. M. "Effect of Electostatic Fields on Free Convection Heat Transfer from Flat Plates," ASME Paper 62-HT-9, ASME-AICHE Joint Meeting on Heat Transfer, Boston, MA, Aug 1963

15. Velkoff, H. R. "Electrofluidmechanics: Investigation of the Effects of Electrostatic Fields on Heat Transfer and Boundary Layers," ASD-TDR 62-650, Aeronautical Systems Division, Air Force Systems Command, WPAFB, OH, 1962

VITA

Major Linn E. Hogue was born ███ ████████ ████ █ ████ ██████ ███████ He graduated from ██████ ██ ██████ ████████████████ in 1968 and entered the University of Oklahoma. He graduated with a Bachelor of Science in Aerospace Engineering in May 1973 from that institution and received a commission in the USAF through the ROTC program. He attended Communications Officer Basic Technical Training in 1974 and served in a number of positions as a Communications Systems Operations Officer, including an 18 month tour as a Wideband Systems Test Engineer. He was awarded a Master of Science in Systems Management from the University of Southern California in 1981. Also in 1981, he was assigned as an Astronautical Engineer with the 6595th Missile Test Group at Vandenberg AFB, California serving as a Missile Flight Test Manager for the Peacekeeper (MX) Ballistic Missile. He entered the School of Engineering, Air Force Institute of Technology in May, 1983.

Permanent Address: ████ ████████ ████████ ██████████████████

REPORT DOCUMENTATION PAGE

1a. REPORT SECURITY CLASSIFICATION	1b. RESTRICTIVE MARKINGS
Unclassified	

2a. SECURITY CLASSIFICATION AUTHORITY	3. DISTRIBUTION/AVAILABILITY OF REPORT
2b. DECLASSIFICATION/DOWNGRADING SCHEDULE	

4. PERFORMING ORGANIZATION REPORT NUMBER(S)	5. MONITORING ORGANIZATION REPORT NUMBER(S)
AFIT/GA/AA/84D-4	

6a. NAME OF PERFORMING ORGANIZATION	6b. OFFICE SYMBOL (If applicable)	7a. NAME OF MONITORING ORGANIZATION
School of Engineering	AFIT/ENY	

6c. ADDRESS (City, State and ZIP Code)	7b. ADDRESS (City, State and ZIP Code)
Air Force Institute of Technology Wright-Patterson AFB, OH 45433	

8a. NAME OF FUNDING/SPONSORING ORGANIZATION	8b. OFFICE SYMBOL (If applicable)	9. PROCUREMENT INSTRUMENT IDENTIFICATION NUMBER

8c. ADDRESS (City, State and ZIP Code)	10. SOURCE OF FUNDING NOS.			
	PROGRAM ELEMENT NO.	PROJECT NO.	TASK NO.	WORK UNIT NO.

11. TITLE (Include Security Classification) see item 19

12. PERSONAL AUTHOR(S)
Linn E. Hogue, B.S., M.S., Major, USAF

13a. TYPE OF REPORT	13b. TIME COVERED	14. DATE OF REPORT (Yr., Mo., Day)	15. PAGE COUNT
MS Thesis	FROM _____ TO _____	1984 December	97

16. SUPPLEMENTARY NOTATION

Approved for public release: IAW AFR 190-17.
LYNN E. WOLAVER   21 Feb 85
Dean for Research and Professional Development
Air Force Institute of Technology (AIC)

17. COSATI CODES			18. SUBJECT TERMS (Continue on reverse if necessary and identify by block number)
FIELD	GROUP	SUB. GR.	Corona Wind; Electrostatic Cooling; Electric Cooling;
20	13		

19. ABSTRACT (Continue on reverse if necessary and identify by block number)

Title: EFFECTS OF THE CORONA WIND ON THE COOLING OF A HORIZONTAL CYLINDER

Thesis Advisor: Milton E. Franke, PhD

Experiments were conducted to determine the effect of the corona wind on the convective heat transfer from a horizontally mounted, heated aluminum cylinder. The cylinder was maintained at ground potential with respect to a positive high voltage emitter. Three types of emitters were used in the testing to create the corona wind: two stretched wires, 0.004 in and 0.0125 in diameter, and a 19 point multipoint emitter. Tests in free convection and with the emitters at various distances and field voltages up to 15 kV were performed to establish a baseline.

20. DISTRIBUTION/AVAILABILITY OF ABSTRACT	21. ABSTRACT SECURITY CLASSIFICATION
UNCLASSIFIED/UNLIMITED ☒ SAME AS RPT. ☐ DTIC USERS ☐	Unclassified

22a. NAME OF RESPONSIBLE INDIVIDUAL	22b. TELEPHONE NUMBER (Include Area Code)	22c. OFFICE SYMBOL
Milton E. Franke, PhD	(513) 255-2362	AFIT/ENY

DD FORM 1473, 83 APR EDITION OF 1 JAN 73 IS OBSOLETE. UNCLASSIFIED

Item 19 continued:

Emitters with and without a metallic mesh grid and a two dimensional wooden shroud, or nozzle, were tested in various configurations over a range of electrostatic field conditions. In addition, the velocity of the corona wind in certain configurations was measured and a blown air system was used to simulate the corona wind with uncharged air to compare their respective effects on the convective heat transfer from the cylinder.

Results show that significant increases (up to 6 times) in convective heat transfer were effected. The grid and shroud in various combinations were not as effective in increasing the heat transfer as the emitters alone. The uncharged air was more effective in increasing the heat transfer from the cylinder than corona wind at the same velocity. The size and type of emitter chosen significantly affected the amount of increase in heat transfer at a particular field voltage.

The parameters varied in the experiments included electrostatic field voltage, emitter to cylinder spacing, emitter to grid spacing, type of emitter, and shroud spacing and position. The primary techniques for data analysis were an energy balance method, and flow visualization with a Mach-Zehnder interferometer.